PSI-PR-92-27
November 1992

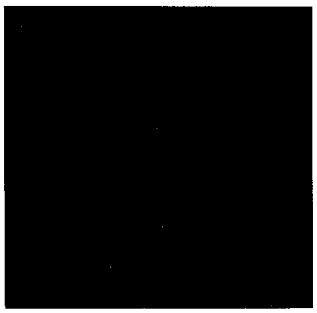

Paul Scherrer Institut

The Static Approximation of Heavy-Light Quark-Systems - A Systematic Lattice Study[1] -

C. Alexandrou[a], S. Güsken[b], F. Jegerlehner[a], K. Schilling[b], R. Sommer[c2]

[a] *PSI, CH-5232 Villigen, Switzerland*
[b] *Physics Department, University of Wuppertal D-5600 Wuppertal 1, Fed. Rep. Germany*
[c] *CERN, Theory Division, CH-1211 Geneva 23, Switzerland*

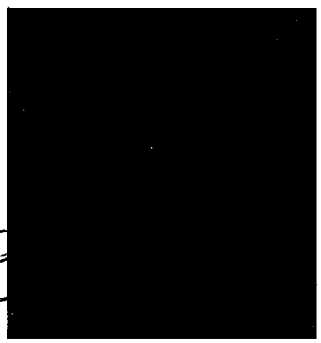

CERN-TH 6692/92
PSI-PR-92-27
WUB 92-34

The Static Approximation of Heavy-Light Quark-Systems - A Systematic Lattice Study[1] -

C. Alexandrou[a], S. Güsken[b], F. Jegerlehner[a], K. Schilling[b], R. Sommer[c2]

[a] *PSI, CH-5232 Villigen, Switzerland*
[b] *Physics Department, University of Wuppertal D-5600 Wuppertal 1, Fed. Rep. Germany*
[c] *CERN, Theory Division, CH-1211 Geneva 23, Switzerland*

Abstract

We present a study of *finite a* and *volume* effects of the leptonic decay constant f of heavy pseudoscalar mesons in the static approximation. This study is performed on a number of lattices at $\beta = 5.74, 6.0$ and 6.26 covering sizes from about $0.7\ fm$ to $2\ fm$. We confirm that beyond $1.5\ fm$ the volume dependence is negligible. By carefully analysing results obtained using different trial wave functions for the heavy meson we find no dependence on the smearing. We also give results for the mass difference of the scalar - pseudoscalar and the Λ_b - pseudoscalar. Using the mass of the pseudoscalar meson we estimate the distance of string breaking in the static quark potential.

[1] work supported in part by DFG grant Schi 257/3-1.
[2] *on leave of absence from University of Wuppertal.*

1. Introduction

There is continued interest in applying the infinite mass effective theory (IMET) [1] to compute properties of heavy-light quark systems in the range of the b- and c-quarks. However the issue of the domain of its validity is still unsettled: it most likely depends on the particular observables under consideration. Lattice methods offer a laboratory to establish beyond which mass the infinite mass limit could be regarded as a good approximation. The lattice formulation of IMET, originally suggested by Eichten [2], has been studied subsequently by a number of authors [3-9]. There are strong indications, that the infinite mass limit of the leptonic decay constant f of the pseudoscalar heavy-light meson needs large corrections to be applicable in the D-meson region. In order to reach a definite conclusion on f and other quantities such as the scalar-pseudoscalar mass splitting Δ_S and the Λ_b - pseudoscalar mass difference Δ_Λ, however, one has to gain better control on various systematic effects of the infinite mass lattice results. There are a number of issues to be addressed such as constraints of finite lattice resolution and extension, finite u and d quark mass and the necessity of renormalisation. In addition one has to bear in mind, that before one can extract any reliable information, one has to achieve ground state enhancement by suitable smearing techniques [3, 4, 10].

In this paper, we intend to consolidate previous static lattice results on f [3, 4] with respect to the error sources mentioned above and to explore the feasibility of studying Δ_S and Δ_Λ. For that purpose, we present in the following a fairly comprehensive analysis, performed on lattices ranging in size from about 0.7 to 2 fm at $\beta = 5.74, 6.0$ and 6.26. Particular emphasis will be given to the pitfalls of ground state projection. We will show that we can safely identify the ground state contributions in the b-quark mesons when smeared interpolating fields are used for the mesons. Using several different interpolating fields we find no dependence of the final result on the type of wave function used. This is what is to be expected and it is contrary to results found in ref. [7].

In order to connect the lattice results to physics, it is important to address finite a and finite size effects as well as renormalisation. We find that the volume effects are negligible beyond lattice sizes of 1.5 fm. Finite a effects turn out to be small when choosing the string tension as the appropriate mass scale. In this way, the most serious source of uncertainty on f remains the perturbative determination of its renormalisation factor Z. Of course all statements that we make here are true within the quenched approximation. We have no way of giving a reliable estimate of the error due to quenching.

The paper is organized as follows: Section 2 will deal with the smearing technique for ground state enhancement using gauge invariant wave functions. Section 3 contains the lattice results on the pseudoscalar mass and leptonic decay constant as well as the mass splittings of scalar-pseudoscalar, Δ_S, and Λ_b-pseudoscalar, Δ_Λ. Their connection to physical quantities is discussed in section 4. The reader not interested in lattice

in lattice technicalities may go directly to section 4. In section 5 we discuss the availability of the physics of string breaking in the environment of quenched computations and give an estimate of the string breaking distance R_b obtained in the quenched approximation. The parameters and technical details characteristic to our simulations are collected for convenience in appendix A.

2. Smearing Techniques

In this work we consider correlation functions of interpolating fields for hadrons that consist of light quarks (l) and one heavy quark (h). The heavy quark is treated in the static approximation with its propagator given by[2,11]

$$\begin{aligned} S_h(x;y) = \delta_{\vec{x},\vec{y}} \ \{ & \ \Theta(x_4 - y_4)\, W^\dagger(\vec{x}; y_4, x_4)\gamma^+ \\ & + \ \Theta(y_4 - x_4)\, W(\vec{x}; x_4, y_4)\gamma^- \}\,, \\ \gamma^\pm = (1 \pm \gamma_4)/2 \quad . & \end{aligned} \tag{2.1}$$

Here $W(\vec{x}; x_4, y_4) = \prod_{t=x_4}^{y_4-a} U_4(\vec{x}, t)$ is the gauge parallel transporter from point $(\vec{x}, x_4)$ to $(\vec{x}, y_4 - a)$. In eq.(2.1), the exponential prefactor $\exp(-|x_4 - y_4|\ m_h)$ has been dropped, since this corresponds only to a common shift of all energy levels by the bare mass of the heavy quark.

In order to connect to physical i.e. renormalisation group invariant quantities within the static approximation, we have to go beyond the formal expression of eq.(2.1). This amounts to taking into account the renormalisation of currents and the effect of the self energy of a static quark which in the continuum limit is divergent. We will discuss this issue in more detail in section 4.1. Given the renormalisation constant of the axial current, Z_{stat}, the physical decay constant f is calculated through the lattice matrix element

$$< 0|\mathcal{M}^{loc,loc}_{\gamma_4\gamma_5}(0)|P >= Z^{-1}_{stat}\ f\sqrt{M_P/2}\ \ a^{3/2} \quad . \tag{2.2}$$

In this equation, all quantities are understood to be in the static approximation. For later use we define

$$\hat{F} = f\sqrt{M_P}\left(\frac{\alpha_s(e^{-2/3}M_P)}{\alpha_s(e^{-2/3}M_B)}\right)^{6/[illegible]} \quad . \tag{2.3}$$

The matrix element $< 0|\mathcal{M}^{loc,loc}_{\gamma_4\gamma_5}(0)|P >$ is independent of the mass of the heavy quark, m_h. The logarithmic mass dependence of $f\sqrt{M_P}$ enters through the mass dependence of Z_{stat}. This logarithmic dependence is cancelled in the definition of $\hat{F}$, which is the proper quantity that has a finite limit as $m_h \to \infty$. The field $\mathcal{M}^{loc,loc}_{\gamma_4\gamma_5}(\vec{x}, t)$ is the time component of the local axial vector current in the general notation

$$\mathcal{M}^{I,J}_{\Gamma}(\vec{x}, t) = \bar{h}^I(\vec{x}, t)\ \Gamma\ l^J(\vec{x}, t) \quad , \tag{2.4}$$

where the indices I, J denote smearing local fields with trial wave functions of type

$$l^J(\vec{x}, t) = \sum_{\vec{y}} \Phi^J(\vec{x}, \vec{y}; \mathcal{U}(t))\ l(\vec{y}, t) \quad , \tag{2.5}$$

and $\Gamma = \gamma_4\gamma_5$ in eq. (2.2). $\Phi^J(\vec{x},\vec{y};\mathcal{U}(t))$ depends in a gauge invariant way on the link variables denoted by $\mathcal{U}(t)$. The case of the local interpolating field that appears in the definition of the decay constant in eq.(2.2) is given by

$$\Phi^{loc}(\vec{x},\vec{y};\mathcal{U}(t)) = \delta_{\vec{x}\vec{y}} \, .$$

In order to calculate the matrix element required in eq.(2.2) one starts from the meson–meson correlation function

$$C_\Gamma^{I,J;K,L}(t) = \sum_{\vec{x}} < \mathcal{M}_\Gamma^{I,J}(\vec{x},t) \; [\mathcal{M}_\Gamma^{K,L}(\vec{0},0)]^\dagger > \quad . \tag{2.6}$$

Due to the positivity of the transfer matrix [12], this has the general representation

$$C_\Gamma^{I,J;K,L}(t) = \sum_{n\geq 1} < 0|\mathcal{M}_\Gamma^{I,J}(\vec{0},0)|n,\gamma >< n,\gamma|\mathcal{M}_\Gamma^{K,L}(\vec{0},0)]^\dagger|0 > \exp(-\tilde{M}_n(\gamma)t) \quad . \tag{2.7}$$

Note that we distinguish between the "masses" $\tilde{M}_n$ in the static approximation, that appear in the above formula and the physical mass of the meson (e.g. M_P) as used in eq.(2.2). Eq. (2.7) gives the formula appropriate for an infinitely large temporal lattice, since for the time extent of about 4 fm used in our simulations, corrections to the infinite limit are expected to be negligible. We have also assumed in this decomposition, that the trial wave functions $\Phi^J(\vec{x},\vec{y};\mathcal{U}(t))$ do not introduce angular momentum and hence the intermediate meson states $|n,\gamma>$ are uniquely labelled by the spin/parity quantum numbers characteristic to Γ and the excitation level n. Due to the additional spin symmetry of IMET [13] we only need to distinguish between pseudoscalar P ($\gamma = \gamma_5$) and scalar S ($\gamma = 1$) particles, the vector being degenerate to the pseudoscalar.

For sufficiently large time separation t, all contributions are exponentially suppressed with respect to the ground state ($n = 1$) in eq.(2.7). Therefore, the matrix element defining f in eq.(2.2) can be obtained by choosing $I,\ldots,L = loc$ referred to as "local-local" correlation function. In the following, we will use the shorthand notations $|1,\gamma_5>=|P>$, $M_1(\gamma_5) = M_P$ and $M_1(1) = M_S$.

Ground state dominance of the correlation function is signalled by the occurrence of a plateau, i.e. the 'local mass'

$$\mu_\Gamma^{I,J;K,L}(t) = \log(C_\Gamma^{I,J;K,L}(t)/C_\Gamma^{I,J;K,L}(t-a)) \quad . \tag{2.8}$$

is t-independent for a range of t. So far, it has been found impossible to attain such a plateau within the static approximation, before the signal is lost in the statistical noise. The situation of our purely local data from lattice D2a (the notation for our lattices being defined in table 1) is depicted by the diamonds in fig. 1. Given the statistical errors it is again not possible to establish the existence of a plateau, up to time separation of $t = 10a$ (or $t \simeq 3.6GeV^{-1}$).

The situation is greatly improved by using appropriate smearing techniques [10]. Translation invariance and the hermiticity of Φ imply the symmetry relations for the

expectation values

$$C_\Gamma^{I,loc;J,loc}(t) = C_\Gamma^{loc,I;loc,J}(t) \quad . \tag{2.9}$$

In other words we can choose whether to smear the light or the static quark in the correlator, without change in the expectation values. Moreover, we have

$$C_\Gamma^{I,loc;J,loc}(t) = C_\Gamma^{J,loc;I,loc}(t) \quad . \tag{2.10}$$

The statistical errors of these quantities, however, do not at all obey such identities! We demonstrate this fact for the second of these equations in fig. 2 where we show a comparison of the 'local masses' obtained from $C_{\gamma_4\gamma_5}^{loc,loc;I,loc}(t)$ and $C_{\gamma_4\gamma_5}^{loc,loc;I,loc}(t) + C_{\gamma_4\gamma_5}^{loc,I;loc,loc}(t)$ for gaussian smearing. There is a dramatic difference in errors between the two cases. So it is much more advantageous to smear the static quark source than to apply smearing to the static sink[3]. The appendix B presents arguments for this empirical error behavior. The difference in error bars shown in fig. 2 amounts to a significant improvement in our ability to localize the plateau[4]. Smearing both heavy and light quarks on lattice C4 at $\beta = 6.0$, we could not do better.

In order to construct the purely local quantity $< 0|\mathcal{M}_{\gamma_4\gamma_5}^{loc,loc}(0)|P >$ from the smeared correlation function $C_{\gamma_4\gamma_5}^{I,J;I,J}(t)$ and $C_{\gamma_4\gamma_5}^{loc,loc;I,J}(t)$, one has first to establish their plateaus as described in eq.(2.8). We fit data showing ground state dominance to the one-exponential expressions

$$\begin{aligned} C_{\gamma_4\gamma_5}^{I,J;I,J}(t) &\simeq |< 0|\mathcal{M}_{\gamma_4\gamma_5}^{I,J}(\vec{0},0)|P >|^2 \exp(-M_P t) \\ &= A\exp(-M_P t) \qquad (2.11) \\ C_{\gamma_4\gamma_5}^{loc,loc;I,J}(t) &\simeq < 0|\mathcal{M}_{\gamma_4\gamma_5}^{loc,loc}(\vec{0},0)|P >< P|\mathcal{M}_{\gamma_4\gamma_5}^{I,J}(\vec{0},0)]^\dagger|0 > \exp(-M_P t) \\ &= B\exp(-M_P t) \qquad (2.12) \end{aligned}$$

and retrieve the local matrix element in form of the ratio $B/\sqrt{A}$.

Clearly the trial wave functions Φ^I and Φ^J have to be constructed such that the excited state contributions are sufficiently suppressed so that the one-exponential behavior in the previous equations can be observed before the statistical noise dominates the signal for both correlators given in (2.11) and (2.12).

To achieve this goal, we have considered three types of wave functions[10]:

1. Gaussian:

$$\Phi^G(\vec{x},\vec{y};\mathcal{U}(t)) = (1+\alpha H)^n(\vec{x},\vec{y};\mathcal{U}(t))$$

with the hopping matrix

$$H(\vec{x},\vec{y};\mathcal{U}(t)) = \sum_{i=1}^{3}(U_i(\vec{x},t)\delta_{\vec{x},\vec{y}-\hat{i}} + U_i^\dagger(\vec{x}-\hat{i},t)\delta_{\vec{x},\vec{y}+\hat{i}})$$

[3]This observation has been made already in ref. [8].

[4]It turns out that for the final determination of the decay constant, however, the statistical error is very similar in the two cases.

that contains the optimisation parameters α and n.

2. Exponential:

$$\Phi^E(\vec{x},\vec{y};\mathcal{U}(t)) = (K\delta_{\vec{x}\vec{y}} - H(\vec{x},\vec{y};\mathcal{U}(t)))^{-1}$$

with the optimisation parameter K.

3. Combinations:

$$\omega\ \Phi^{loc}(\vec{x},\vec{y};\mathcal{U}(t)) + \Phi^G(\vec{x},\vec{y};\mathcal{U}(t)).$$

Let us briefly discuss some features of these wave functions:[5]

All wave functions are defined local in time which means that they involve gauge fields only in one time slice and are gauge covariant. The first property is needed in order that eq. 2.7 holds. The second one insures that no problems due to gauge fixing occur. Such problems could arise, for example, due to noise originating from incomplete gauge fixing. In addition, the necessity to work in the Coulomb gauge for all other wave functions that have been suggested [14] means that a significant amount of numerical effort is spent in the gauge fixing procedure. The gaussian wave function given above is therefore comparatively cheap to compute.

The exponential wave function needs the calculation of a 3-dimensional scalar propagator through the solution of a linear equation. We refer to it as an exponential wave function because the $\vec{x}-\vec{y}$ dependence in the non-interacting case ($U_i(\vec{x},t)=1$) is of Yukawa-type. This particular wave function was found [3] to be very effective in projecting onto the ground state at relatively small β ($\beta \simeq 5.7$). In our new simulations, we have switched to using the gaussian wave function (this notation originates again from its dependence on $\vec{x}-\vec{y}$ in the free case), because it is numerically much cheaper. As we will demonstrate in the following, the two wave functions are equally good in projecting onto the ground state around $\beta = 6.0$ and for $\beta = 6.26$ the gaussian wave function achieves very early ground state dominance. Although Φ^E has not been tried out at this β value, we expect Φ^G to be superior in ground state projection.

In our previous calculation we tuned the parameter(s) in the wave function to obtain early plateaus in the smeared-smeared *and* local-smeared local masses. Defining

$$r_2^2 = < \frac{\sum_{\vec{x}} \vec{x}^2 \mathrm{Tr}[\Phi^J(\vec{x},0)(\Phi^J(\vec{x},0))^\dagger]}{\sum_{\vec{x}} \mathrm{Tr}[\Phi^J(\vec{x},0)(\Phi^J(\vec{x},0))^\dagger]} > \qquad (2.13)$$

the optimisation of the wave functions coincided with an r.m.s. radius r_2 of approximately 0.3 fm. This is quite a reasonable size for a hadronic wave function.

[5] Additional aspects are discussed in an early investigation [10].

3. Signals from the Lattice

3.1 Pseudoscalar Mass and Decay Constant

As we already pointed out, smearing of the quark fields is crucial for filtering the ground state before noise sets in. Needless to say, the results must be independent of the details of the applied smearing. This issue has been addressed already in the first calculations of $\hat{F}$ in the static approximation [3, 5], where different wave functions were reported to render consistent results. More recently ref. [7] supposedly revealed a systematic dependence of $\hat{F}$ on the wave function size, particularly at larger values of β. In order to settle this question, we performed a careful analysis on wave function dependence at $\beta = 6.26$. We used a $18^3 \times 48$ lattice (denoted by $D2a$ in table 1), and six different wave functions, whose parameters are listed in table 2. The first three wave functions are constructed using a combination of a local and a gaussian wave function with $n = 100, \alpha = 4$. The remaining three represent pure gaussian smearing. To convey a physical idea of the involved sizes we quote the r.m.s radii r_2 (defined in eq.(2.13)) as well as the radii r_1 (defined as in eq.(2.13) but with $\vec{x}^2$ replaced by $|\vec{x}|$). As can be seen from table 2, r_2 is varied within $3.9a \leq r_2 \leq 6.5a$.

The impact of smearing on the t-dependent masses, as derived from $C^{I,loc;J,loc}_{\gamma_4\gamma_5}$ ("smeared - smeared") is demonstrated in fig.1. We can clearly ascertain a universal plateau, independent of the particular wave function chosen. Approximate ground state dominance sets in as early as $t = 2a$. Fits to eq.(2.11) in the t-range of the plateau yield consistent mass values, as can be seen from table 2[6].

Since the smeared-smeared correlation function is convex (cf. eq. (2.7)), we were able to identify its ground state plateau rather unambiguously. The evaluation of local-smeared correlation functions, on the other hand, poses a more serious problem, as they do not share this convexity property. We show their t-dependent masses in fig. 3: without prior knowledge of the height of the plateau (and in particular with the larger error bars in the t-dependent masses obtained in ref. [7]), one is liable to misidentify the position of the plateau and thus to end up with wave function dependent results. It is therefore important to ensure that the plateau has the same height for both local-smeared and smeared-smeared correlators. For this purpose, we have inserted into fig. 1 and 3 the plateau as obtained from a fit to smeared-smeared correlators. (using the best wave function with $\alpha = 4$, $n = 100$). Although the t-dependent masses

[6]Fig. 1 shows quite a strong scatter in the data at intermediate and large values of t. We investigated this in some detail: The error estimates of the t-dependent masses were calculated using the covariance matrix. One may suspect that the off diagonal elements of the covariance matrix in themselves are not estimated accurately enough, leading to unreliable error estimates in the t-dependent masses. To check this suspicion, we estimated the *error of* the error with the jackknife procedure and found it to be only of the order of 15%, in agreement with a gaussian distribution. Furthermore no signs of significant autocorrelations were revealed by the data (using binning). We conclude that the reason for the scatter in fig. 1 is that correlations over more than one time-slice are not strong. This fact actually improves the errors for the mass from the smeared-smeared correlators: different patches of t contribute independent information.

depend substantially on the underlying wave functions, they finally end up in the same plateau!

So it is obvious that the evaluation of smeared correlators has its pitfalls. An appropriate procedure to determine $\hat{F}$ is to first determine the ground state mass from the smeared-smeared correlator and then to inject it into a constrained fit of the local-smeared correlator. These fits, done in the region of the respective plateaus yield consistent results. This is demonstrated in table 2, where the resulting values for $\hat{F}$ are given for all six wave functions as a function of t_{min}, the minimum time separation used in the fit to the local-smeared correlator. The stability of $\hat{F}$, under variations of the wave function and t_{min}, is remarkable. We therefore corroborate our previous conclusion [15] that there is no spurious dependence of $\hat{F}$ on the size of the wave function.

In addition, we have tried an alternative procedure, based on the relation

$$C^{I,J;loc,loc}_{\gamma_4\gamma_5}(t) \;/\; \sqrt{C^{I,J;I,J}_{\gamma_4\gamma_5}(t)} \sim < 0|\mathcal{M}^{loc,loc}_{\gamma_4\gamma_5}(0)|P > \exp(-\tilde{M}_P\, t/2) \quad , \qquad (3.1)$$

which holds in the region where both correlation functions on the l.h.s. show ground state dominance. Performing fits to this ratio, we obtain results consistent with those from the method described above. But the statistical errors are larger, because one has to exclude part of the plateau of the smeared-smeared correlator from the analysis[7].

Let us finally mention that the optimal wave function ($\alpha = 4,\ n = 100$) carries an r.m.s. radius of about $0.3fm$, in agreement to earlier findings [3].

In completing our systematic study on the smaller lattices, we restrict ourselves to the use of optimal wave functions, with $r_2 \simeq 0.3fm$. In fig. 4 we show the t-dependent masses from the local-smeared correlators for the lattices A3, C3 and D2a corresponding to the β values of 5.74, 6.0 and 6.26. Note that the data points again converge into their respective errors bands, as determined from fits to the smeared-smeared correlators. The numerical results for all the lattices are collected in table 3. Here we quote values on $\tilde{M}_P$ and $\hat{F}$ as well as indicate their stability with respect to different fit ranges in t, at various quark masses and β values. By looking at these numbers, we conclude that the results for $\hat{F}$ and $\tilde{M}_P$ are again fairly insensitive to the wave functions chosen, once the fit region is appropriately identified: a variation of the lower cut t_{min} in the fitting procedure renders results for $\hat{F}$, that become stable, as soon as t_{min} lies within the plateau. In addition, we stress the agreement of the results for lattices A3 with A3a and C3 with C3a respectively. The old calculations [3] on A3a and C3a had been done with the exponential wave function, whereas the results on A3 and C3 are obtained with Φ^G. We find a beautiful stability of the results with respect to the *shape* of the wave function. Furthermore, Φ^E gives earlier plateaus at $\beta = 5.74$ but at $\beta = 6.0$ no clear difference is visible. This, together with the early plateaus achieved at $\beta = 6.26$, indicate that Φ^G is the better choice at larger β, a feature that is very welcome, given the low numerical cost of constructing Φ^G.

[7] A third possibility that has been discussed in ref. [5] differs only slightly from the method used here.

3.2 Mass splittings

We start with the determination of the mass difference between the scalar and pseudoscalar states,

$$\Delta_S = \tilde{M}_S - \tilde{M}_P = M_S - M_P \quad . \tag{3.2}$$

For the scalar state we will discuss results that have been obtained with the interpolating field $\mathcal{M}_1^{I,J}(\vec{x},t)$ from eq.(2.4). In order to reduce statistical and systematic errors the mass difference, in most cases, is determined directly from an analysis of the ratio of the respective correlators:

$$R_S^{I,J}(t) = C_1^{I,J;I,J}(t) \;/\; C_{\gamma_4\gamma_5}^{I,J;I,J}(t) \tag{3.3}$$

We find that the scalar ground state signal is somewhat inferior to the respective pseudoscalar signal. We note in passing that we have attempted to improve signals by using another operator to excite the scalar state: In the non-relativistic quark model, the scalar state is a p-wave excitation. We therefore tested in addition an interpolating field $\mathcal{M}_{\gamma_4\gamma_5}^{P,loc}(\vec{x},t)$ with a p-wave trial wave function Φ^P which is constructed by applying a covariant (lattice-) derivative to the wave functions from sect. 3.2. The latter method produced consistent results, but with larger statistical errors.

The t-dependent masses from smeared-smeared correlators as derived from $R_S^{I,J}$ are plotted in fig. 5. The x-axis is scaled to physical units using the string tension. Comparing results obtained at different volumes, the figure demonstrates that finite size effects are negligible for Δ_S. We find first evidence of plateaus in the regions $t\sqrt{\sigma} \geq 1$ for $\beta = 5.74$ and $t\sqrt{\sigma} \geq 0.7$ for $\beta = 6.0$ and $\beta = 6.26$. However due to the early noise dominance, the situation is not as clean as in the case of the pseudoscalar yielding to a larger uncertainty in the determination of Δ_S. The numbers for Δ_S, as obtained from a one-term exponential fit to eq.(3.3), are quoted in table 4. In a few cases where the plateau for R_S was very limited we fitted separately the two channels to have at our disposal somewhat larger plateaus at a price of larger error bars. These fits are indicated by the daggers in table 4.

In an analogous way, we can determine the mass difference between the Λ_b and the B-meson

$$\Delta_\Lambda = \tilde{M}_\Lambda - \tilde{M}_P = M_\Lambda - M_P. \tag{3.4}$$

The form of the Λ-correlator reads

$$D^{I,J}(t) = \sum_{\vec{x}} < Tr\{\gamma^+ \mathcal{B}^{I,J}(\vec{x},t)\; [\mathcal{B}^{I,J}(\vec{0},0)]^\dagger\} > \quad , \tag{3.5}$$

where the Λ-operator $\mathcal{B}$ is defined by

$$\mathcal{B}_\alpha^{I,J}(\vec{x},t) = \sum_{a,b,c,\alpha,\beta,\gamma} \epsilon_{abc}\; (h^I(\vec{x},t))_\alpha^a\; (u^J(\vec{x},t))_\beta^b\; (C\gamma_5)_{\beta\gamma}\; (d^J(\vec{x},t))_\gamma^c \quad . \tag{3.6}$$

Here a,b,c (α,β,γ) denote color (Dirac) indices and C is the charge conjugation matrix. The field $\mathcal{B}_\alpha^{I,loc}(\vec{x},t)$ is to be interpreted as a diquark trial wave function for the

baryon: the two light quark fields are restricted to be local with respect to each other. Otherwise $\mathcal{B}_\alpha^{I,J}(\vec{x},t)$ amounts to a general wave function ansatz. In ref. [16] where the mass of Λ_b was computed a diquark type of wave function was used.

Like in the case of Δ_S, we avoid computing the mass splitting by separate analysis of the individual correlators, but rather consider their ratio

$$R_\Lambda^{I,J}(t) = D^{I,J}(t) \;/\; C_{\gamma_4\gamma_5}^{I,J;I,J}(t). \tag{3.7}$$

We plot the t-dependent mass-splitting arising from $R_\Lambda^{I,J}(t)$ in fig. 6, where both axis are scaled to physical units using, as in fig. 5, the string tension. This means that all data should, apart from scaling violations, merge into one and the same plateau. The data are consistent with scaling, but the statistical errors are obviously too large to make a definite case. Note that the t-dependent mass-splitting for $\beta = 6.26$ where a diquark trial wave function is used starts off very high. The effect is due to the numerator in eq.(3.7). Therefore the underlying diquark type trial wave function achieves a small overlap with the ground state. The other trial wave functions appear to do better.

In table 4, we have included the results arising from one-term exponential fits to eq.(3.7). The fits were done in the t-ranges where the t-dependent mass-splittings are consistent with a plateau. We stress, however, that the existence of these plateaus is still debatable. In order to settle this issue more effort must be spent to optimize the wave functions.

4. Connecting to Physics

4.1 The Renormalisation Problem

We have encountered various quantities in the static approximation on the lattice, whose physical significance has to be elucidated. The most questionable quantity is the "pseudoscalar mass" $\tilde{M}_P$, as it carries a linear divergence, due to the self energy. In this section we will first investigate whether lowest order effective coupling perturbation theory allows to extract this linear divergence. If this worked out, one would be able to produce meaningful numbers on the binding energy B from static lattice calculations. Another important issue is the renormalisation factor Z_{stat} for the axial current. We are going to consider the possible improvement on this perturbatively computed quantity, by employing a renormalised coupling.

Binding energy. We start by splitting up the mass into the binding energy B and the divergent self energy $E(a)$:

$$\tilde{M}_P = E(a) + B \quad . \tag{4.1}$$

An estimate for the self energy may be obtained in perturbation theory, with the lowest non-trivial order term being linearly divergent

$$E(a)|_{pert} = \frac{1}{a}(\frac{2}{3}G(\vec{0})\tilde{g}^2 \; + \; O(\tilde{g}^4)), \tag{4.2}$$

$$G(\vec{0}) = \int_{-\pi}^{\pi} \frac{d^3k}{(2\pi)^3} \frac{1}{4\sum_j \sin^2(k_j/2)} = 0.253(1) \quad .$$

The coupling in eq. (4.2) should be taken at the scale of the cutoff a^{-1}. It has been suggested [17] that a more suitable expansion parameter than the bare coupling, $g_0^2 = 6/\beta$, at this scale is given by

$$\tilde{g}^2 = g_0^2 / < \frac{1}{3}\mathrm{TrP}_{\mu\nu} > \quad . \tag{4.3}$$

In addition one observes [18], that the g^4 terms of the perturbative expansions of several short distance quantities are much smaller in an expansion in terms of $\tilde{g}^2$ as compared to an expansion in terms of g_0^2, which points to a better convergence of the former expansions. Finally, it has been shown that indeed the 1-loop relation between $\tilde{g}^2$ and $g^2_{\overline{MS}}$ is quite accurate in SU(2) pure gauge theory [19]. It should be noted, moreover, that the use of an effective coupling similar to eq. (4.3), in the perturbative expansion of the β-function, amounts to a considerable reduction of subasymptotic contributions to the string tension [20]. Therefore, to present knowledge, $\tilde{g}^2$ is the appropriate coupling to be used in the perturbative expansion eq. (4.2).

It remains to be checked, however, whether a perturbative estimate of $E(a)$ is sufficient to extract the binding energy B. This can be done by looking at the resulting estimate of the binding energy [8]:

$$\tilde{B} \equiv \tilde{M}_P - E(a)_{pert} \quad . \tag{4.4}$$

It should exhibit scaling behavior, up to terms of order $O(a)$. Using data from table 3 we obtain for the dimensionless ratio $\tilde{B}/\sqrt{\sigma}$ the values 1.40(2), 1.80(6), and 1.98(6) at $a\sqrt{\sigma} = 0.38$, 0.22, and 0.151, respectively. As the observed variation of $\tilde{B}$ might still constitute a large $O(a)$ effect, we have in addition computed the quantity

$$(V_0 - 2\; E(a)|_{pert})/\sqrt{\sigma} \quad ,$$

with V_0 the constant piece of the heavy quark potential defined in eq. (4.9) and given in table 5. It should also be independent of a if $E(a)|_{pert}$ is a good approximation to the divergent self energy of a static quark. In this case the corrections should be smaller - of order $O(a^2)$. Here, the numbers read $(V_0 - 2\; E(a)|_{pert})/\sqrt{\sigma} = 0.008(16)$, 0.28(3), and 0.56(2) to be compared to $V_0/\sqrt{\sigma} = 1.70$, 2.81, and 4.02, respectively.

[8] It should be noted that eqs. (4.1) and (4.2), are expected to hold at most for an intermediate range of lattice spacings, since, as one approaches the continuum limit $a \to 0$; $\tilde{g}^2 \to 0$, possible non-perturbative terms in eq. (4.2) become increasingly more important when they are inserted into eq. (4.4).

We conclude that on this level there is no justification whatsoever to estimate $E(a)$ by lowest nontrivial order perturbation theory.

We have discussed this issue in some detail in view of the recent proposal to simulate heavy quark systems with a nonrelativistic effective Lagrangian [21]. In practice [22, 23], the coupling constants in this effective Lagrangian are estimated from perturbation theory to first order in $\tilde{g}^2$. They are divergent like $E(a)$. The above considerations cast considerable doubt on the validity of such a procedure or at least call for a serious estimate of systematic errors introduced through the uncertainties in the coupling constants in the effective Lagrangian.

As a result, we have to refrain from quoting any number for the binding energy in a static–light meson. On the other hand, in mass splittings like Δ_S and Δ_Λ, the self energies cancel and we obtain relevant estimates that are good to lowest order in $1/m_h$.

Decay constant. We turn next to the question of optimizing, within a given order, the perturbative renormalisation factor Z_{stat}. This quantity is implicitly defined [24, 25] by matching the continuum (full theory) axial vector correlation function $C_{A_0}(t)$ at large euclidean time separation t with its lattice counterpart $C^{loc,loc;loc,loc}_{\gamma_4\gamma_5}(t)$:

$$C_{A_0}(t)e^{M_H t} = Z^2_{stat}(a, m_h)e^{\tilde{M}_P t}C^{loc,loc;loc,loc}_{\gamma_4\gamma_5}(t)\ (1 + O(1/m_h)) \quad . \tag{4.5}$$

Since eq.(4.5) has to hold also in the range of intermediate time separation t, the renormalisation constant Z_{stat} can be calculated in perturbation theory:

$$Z^2_{stat}(a, m_h) = e^{(M_H - \tilde{M}_P)t}\frac{C^{loc,loc;loc,loc}_{\gamma_4\gamma_5}(t)}{C_{A_0}(t)}|_{pert} \quad . \tag{4.6}$$

$M_H - \tilde{M}_P = m_h - E(a)$ has to be determined in perturbation theory only to remove the t–dependence of the r.h.s. and there is no linear divergence in Z_{stat} [25].

The result is:

$$Z_{stat}(a, m_h) = 1 + \frac{g^2}{4\pi}(\frac{1}{\pi}\log(a\ m_h) - 2.372) \quad . \tag{4.7}$$

This is a first order perturbative result and it is not *a priori* clear which coupling should be used in eq. 4.7. It is common practice (see ref. [25] and references therein) in numerical estimates of eq.(4.7) and hence of $\hat{F}$ to use the bare coupling g_0^2 as this choice seems to be natural in connection with lattice regularisation. However, the expansion in the coupling constant has to approximate a physical correlation function both in the continuum (left hand size of eq. (4.5)) and on the lattice (right hand size of eq. (4.5)). As we have already pointed out in connection with eq. (4.3) g_0^2 is not a good expansion parameter and should be replaced by a renormalised coupling constant defined by some physical process [18] . We may use the $\overline{MS}$ coupling at a suitable scale which is known to give well behaved expansions for many physical quantities. For this purpose we have to estimate the appropriate scale and establish the relationship between $g^2_{\overline{MS}}$ and g_0^2. To estimate the appropriate scale in eq. (4.7) we note that eq. (4.6) is valid for $t >> 1/m_h$, due to the expansion in $1/m_h$. On

the other hand, the time separation is required to be small compared to a typical non-perturbative scale, such that the correlation functions can be approximated by perturbation theory. This sets the requirement $t << 0.5fm$. For $m_h = O(m_b)$, these requirements don't leave much of a window and we conclude that the coupling constant should be evaluated at a scale of about 3 GeV. An estimate for this coupling in pure SU(3) gauge theory is given by [18]

$$g^{-2}_{\overline{MS}}(\frac{\pi}{a}) = g_0^{-2} < \frac{1}{3}\mathrm{TrP}_{\mu\nu} > +0.02461 \quad . \tag{4.8}$$

This refers to the $\overline{MS}$ coupling in the continuum of the pure SU(3) gauge theory. The corresponding expression has been shown to be rather accurate at values of the lattice spacing $a^{-1} = 4\mathrm{GeV}$ in the pure SU(2) gauge theory [19]. As input into eq.(4.8) we need, in principle, an estimate for the lattice spacing at a small value of the bare coupling constant. Using the values for the string tension in table 5 (and for the larger β, the 2-loop renormalisation group equation) we obtain consistently

$$g^2_{\overline{MS}}(3GeV) = 1.9(1) \quad ; \quad Z_{stat}(a, m_h) = 0.71 + 0.048(\log(am_h) - 1.43) \quad .$$

Let us estimate roughly the uncertainty of this renormalisation constant. The logarithmic correction varies only by ± 0.007 over our range of lattice spacings at $m_h = 4.6GeV \simeq m_b$. Varying the argument of $g^2_{\overline{MS}}$ between 1.5 GeV or 9 GeV produces a maximal change in Z_{stat} of ± 0.08. This range also covers changes arising from using a different quantity like the ρ-mass to set the scale and a change to other renormalised couplings like g^2_{MS} or a coupling defined from the force between heavy quarks [20] [9].

4.2 Setting the Scale

We obtain physical results by forming dimensionless ratios, determining their value through the simulation and identifying one quantity with its experimentally measured value. In this way, a reference scale enters. Within the quenched approximation, a natural choice is the *string tension* σ, since it does not involve an extrapolation in quark mass. It carries the disadvantage, though, that it can only be determined from experiments in a rather indirect way.

String tension calculations in lattice gauge theory mainly bear two sources of systematic errors. Firstly the individual values of the potential are determined at finite values of the euclidean time separation, which makes them prone to pollution by "excited states". This error is presumably smaller [26, 27] than the statistical errors of the measurements used here. Secondly the potential parameters are determined from fits within a certain range of the quark separation R. In order to study scaling violations effects, it is crucial to use potential parameters, that have been obtained from fits to a definite parametrisation and fit range in physical units. Here, we follow the philosophy of employing the data from ref. [26] and [27], and restricting ourselves to the range

[9] Note, however, that this range does not include the bare coupling constant.

$0.3\ fm \leq \mathrm{R} \leq 1.0\ fm$[10]. In the following, we use results for σ extracted from fits done with one assumption on the subleading term, namely the one suggested by the bosonic string picture [28]:

$$a\ V(\vec{R}) = aV_0 - \frac{\pi^2}{3} G(\vec{R}/a) + a\ \sigma\ R, \quad R = |\vec{R}|, \quad for\ R\sqrt{\sigma} > 0.3 \tag{4.9}$$

In the R-range given in eq. (4.9), such a parametrisation of the potential is in agreement with all existing lattice simulation results.

Apart from the direct results obtained in simulations, table 5 contains interpolated values for $\beta = 5.74$ and 6.26. For these two β values, $V_0 a$ and $\log(\sigma a^2)$ have been interpolated linearly in β using the two neighbouring Monte-Carlo results. Some uncertainty due to possible deviations from such behavior has been taken into account. Using the values collected in table 5 we can thus express all lattice quantities in physical units.

A second choice for setting the scale is the mass of the ρ resonance M_ρ. Before the ρ mass can be utilized to set the scale, its lattice prediction has to be extrapolated into the chiral regime, however. On the lattice, an accurate computation of M_ρ has been performed in the quenched approximation at $\beta = 5.7$, $\beta = 6.0$ and $\beta = 6.3$ by the APE group [29]. Our own determinations are listed in table 6: $M_\rho a = 0.534(11)$, 0.341(15) and 0.208(15) at $\beta = 5.74$, 6.0 and 6.26 respectively. The $\beta = 6.00$ value is in perfect agreement with the result of ref. [29], although we have used a significantly smaller lattice.

Extrapolation in Quark Mass. For completeness, we will now present some details on quark mass extrapolation. One makes a linear ansatz for the vector meson mass

$$a\ M_V(l,l') = B + C\ (\frac{1}{2\kappa} + \frac{1}{2\kappa'} - \frac{1}{\kappa_c}) \quad . \tag{4.10}$$

The critical value κ_c follows from the relation

$$a^2\ M_P^2(l,l') = A\ (\frac{1}{2\kappa} + \frac{1}{2\kappa'} - \frac{1}{\kappa_c}) \tag{4.11}$$

suggested by lowest order chiral perturbation theory [30]. By l and l' we denote quantities obtained using correlators of light quarks. Here, κ_c differs from its free value of 1/8 because of the explicit breaking of the chiral symmetry in the lattice regularisation [31]. Our fits to eq. (4.11) are shown in fig. 7, for degenerate and non-degenerate light quark masses. The linear dependence of both $M_P^2(l,l')$ and $M_V(l,l')$ on the quark masses is very well satisfied. The κ values corresponding to the up and down quark (κ_u) and to the strange quark (κ_s) can be extracted from

$$A\ (\frac{1}{\kappa_u} - \frac{1}{\kappa_c})/(\sigma a^2) = (137 MeV/420 MeV)^2$$

[10]We are aware of the effects from the subleading terms and other overall uncertainties due to the parametrisations used. We expect that they have little impact on the size of scaling violations, however.

and

$$A\,(\frac{1}{2\kappa_s}+\frac{1}{2\kappa_u}-\frac{1}{\kappa_c})/(\sigma a^2)=(494MeV/420MeV)^2$$

when the string tension σa^2 is used to set the scale (with analogous expressions when scaling with $M_\rho a$). In addition, we quote results for a large number of L and a values, computed at a quark mass m_{2s} of approximately twice the strange quark mass defined by $M_P^2(l,l)/\sigma = 4$. They do not require any extrapolation, but only a mild interpolation in the case of the $\beta = 6.26$ data.

In table 6 we list our results for the vector meson mass at κ_c and κ_s. Tables 7 and 8 give the values, after linear extrapolations to zero quark mass and to m_s[11], for the bare decay constant and mass-splittings, respectively.

As we will base our analysis in the following on the scales extracted from the string tension and the ρ-mass, we briefly investigate, in how far we can expect consistent results from these two scales. Figure 8 shows the ratio $m_\rho/\sqrt{\sigma}$ as a function of the lattice spacing. Perturbative arguments suggest that the dependence of physical ratios on the lattice spacing is linear in the case of the Wilson action[12]. A linear extrapolation in the lattice spacing is shown in the figure. The result at $a = 0$ is some 10% low from the experimental value of 1.75-1.83.

Let us comment finally on the possibility to base the scale on the π decay constant. Our data for f_π show non-linear behavior in the quark mass. Recent calculations of f_π have been able to reach smaller quark masses with good precision and can therefore be extrapolated [32]. Within errors, $f_\pi a$ and $M_\rho a$ give the same lattice spacing at $\beta = 5.8$ and 6.0. The situation for our data is demonstrated in fig. 9. Taking into account the uncertainty in the perturbative renormalisation of f_P, which is not included in fig. 9, we see that the Monte Carlo results for f_P/M_V are consistent with the experimental numbers and therefore the lattice spacings agree within errors. We therefore use exclusively the string tension and the ρ mass to convert our results to physical units.

4.3 Finite Size Scaling

In fig. 10 we plot $\hat{F}/Z_{stat}$ as a function of the spatial lattice length L, both in units of the string tension, at quark mass m_{2s} twice the strange quark mass. We wish to make two comments on the finite size behavior of these data:
1. As the entries into fig. 10 are statistically independent, an alternative search for possible a−effects may proceed via a global fit to the L-dependence. The latter is exponential, with a characteristic decay given by the mass of lowest lying glueball, which winds around the periodic volume. Since $m_{0^{++}}/\sqrt{\sigma} \simeq 3.5$ [33], the sensitivity of our computer experiment is much too low to exploit this.

[11]The values of these quantities at m_{2s} can be directly obtained from tables 3 and 4.

[12]It should be remembered, that this is a perturbative argument. It is in no way obvious that this behavior is the same for long-distance, nonperturbative quantities.

2. One might speculate that the finite size effects seen within the intermediate regime of fig. 10 originate from a distortion of the light-quark wave function in the finite volume. For an exponentially decaying wave function, the finite size effects on the wave function at the origin are again exponential in L. The characteristic scale in this domain is the coefficient in the falloff of the wave function. A rough estimate is given by 1.5 in units of the string tension [34]. We find that the data in fig. 10 can indeed be fitted with the form $\hat{F}\sigma^{-3/4} = 3.64(8) - C\exp(-1.5\sqrt{\sigma}L)$ with a $\chi^2/DoF = 8/9$, if the error of the most precise point is increased to lie in the general ballpark of ± 0.15.

From the above observations we may conclude that within a precision of about 10 percent one can neglect finite size effects on $\hat{F}\sigma^{-3/4}$, in the range $\sqrt{\sigma}L \geq 3$. This remains true also for smaller quark masses, as can be seen by looking at the entries in table 3 for the lattice A3, A3a and A5. We therefore assume that finite size effects are negligible beyond $\sqrt{\sigma}L \geq 3$ for the light quark masses considered here and we proceed to analyse our results in more detail at $\sqrt{\sigma}L \simeq 3$.

Fig. 11 shows the a-dependence of the bare decay constants at the s quark mass and at the u quark mass with both setting the scale through $\sqrt{\sigma}$ and M_ρ. Putting in the value $Z_{stat} = 0.71(8)$ we obtain

$$\hat{F}_s = 0.61(4)(7)GeV^{3/2}, \quad \hat{F}_u = 0.53(5)(6)GeV^{3/2} \tag{4.12}$$

with $\sqrt{\sigma}$ and

$$\hat{F}_s = 0.67(18)(7)GeV^{3/2}, \quad \hat{F}_u = 0.59(18)(6)GeV^{3/2} \tag{4.13}$$

from the M_ρ-scale. The values given in eq. 4.12 and 4.13 are in perfect agreement, with the latter ones having very large errors. The first errors given above are statistical and the second result from our estimated uncertainty of Z_{stat}. We have not included an error for the extrapolation, since our data points at the smallest value of a are within the error bar of the extrapolated values.

From eq. 4.12 we obtain the IMET lattice predictions for the decay constants of B-mesons evaluated in the *static approximation*

$$f_{bs} = 266 \pm 22 \pm 26 \ \ MeV \qquad\qquad f_{bu} = 230 \pm 22 \pm 26 \ \ MeV. \tag{4.14}$$

The central value is significantly lower than the ones of the first calculations [3, 5]. Firstly, there is a significant a-dependence when the scale is set by the ρ-mass, as anticipated in ref. [4]. Secondly, as we explained in section 4.1 the use of *renormalised* perturbation theory in the determination of Z_{stat} decreases the value of the decay constant by about 13%.

For the D-meson one definitely needs the $1/M_P$ correction since by stretching the validity of IMET down to the charm mass, we obtain the extremely high values of

$f_{cu} = 359(34)(39)$ and $f_{cs} = 405(27)(46)$ MeV which contradict results both from lattice calculations with fully propagating quarks and from sum rule evaluations [35].

If one looks at the analogue of fig. 10 for the 1P - 1S splitting, Δ_S, one observes a significant scatter in the data coming from different β's. This indicates that $\Delta_S/\sqrt{\sigma}$ has a stronger a-dependence than the decay constant. Looking at the results given in Table 4, however, we find no significant finite size effects for $L\sqrt{\sigma} \gtrsim 2$ on the level of our statistical uncertainties. Therefore, we can extract the splitting directly at $L\sqrt{\sigma} \simeq 3$. In fig. 12, we show the a-dependence of Δ_S at quark mass m_{2s}. The linear extrapolation to the continuum gives 344(37) MeV from fig. 12a and 383(72) MeV from fig. 12b. At smaller quark masses, our results are too inaccurate to allow for such an extrapolation. We note, however, that no significant quark-mass dependence was observed for this splitting.

Unfortunately a similar analysis is not feasible at the moment for the Baryon-Meson splitting, Δ_Λ. The best we can do, is to take figure 6 as an indication that there is a plateau at $\Delta_\Lambda/\sqrt{\sigma} \simeq 1.5$. This produces a rough estimate of 600MeV for the Λ_b – B-meson mass splitting. Much more work is needed to check the existence of plateaus, the a-dependence, quark-mass dependence and finite size effects for this quantity.

5. String Breaking

We turn now to another observable that may be calculated from our simulation results. It is of interest, because it gives information about the forces between static charges in the *full* theory, i.e. it is a quantity calculated in the quenched approximation which can provide information about $q\bar{q}$ forces with dynamical fermions. In full QCD simulations the breaking of the QCD string, i.e. the flattening of the heavy quark potential at large distances, has been searched for some time. No effect was found in the most serious effort [36]. In the following, we estimate the distance R_b, where the full QCD potential flattens off using only quantities calculated in the quenched approximation [15].

Consider a large Wilson loop $W(\vec{R},T)$, with $T >> R$, in full QCD. It has a representation in terms of the eigenvalues of the QCD-hamiltonian (or transfer matrix):

$$W(\vec{R},t) = \sum_{n\geq 0} |c_n^W(\vec{R})|^2 \exp(-V_n(\vec{R})t) \quad . \tag{5.1}$$

Here $\exp(-V_n(\vec{R}))$ are the eigenvalues of the transfer matrix in the corresponding charged sector of the Hilbert space: the states in this sector transform under gauge transformations according to the 3-representation at position $\vec{0}$ and according to the $\bar{3}$-representation at position $\vec{R}$. The same states contribute in the spectral decomposition of the correlation function

$$\begin{aligned} H(\vec{R},t) &= < \mathcal{M}^{loc,J}_{\gamma_4\gamma_5}(\vec{0},t)\ [\mathcal{M}^{loc,J}_{\gamma_4\gamma_5}(\vec{R},t)]^\dagger \mathcal{M}^{loc,J}_{\gamma_4\gamma_5}(\vec{R},0)\ [\mathcal{M}^{loc,J}_{\gamma_4\gamma_5}(\vec{0},0)]^\dagger > \\ &= \sum_{n\geq 0} |c_n^H(\vec{R})|^2 \exp(-V_n(\vec{R})t) \quad . \end{aligned} \tag{5.2}$$

The ground state potential $V(\vec{R}) = V_0(\vec{R})$ can therefore be called a static quark potential or a static meson potential. Physically, the first interpretation is sensible at relatively short distances, whereas the second one is the appropriate language for large distances (compared to the confinement scale). This can even be put into a quantitative relation: we expect $|c_0^H(\vec{R})|^2 << |c_0^W(\vec{R})|^2$ at small distances and $|c_0^H(\vec{R})|^2 >> |c_0^W(\vec{R})|^2$ at large distances. Furthermore, at large distances, the potential will approach a constant up to non-leading terms (Yukawa-type interactions), because the correlation function factorises:

$$log[H(\vec{R},t)] = log[(C_{\gamma_4\gamma_5}^{loc,J;loc,J})^2] + O(\exp[-m_\pi R]t/R) \quad . \tag{5.3}$$

Simulation results of full QCD [36] indicate, that the QCD-potential is approximated rather well by the quenched potential out to relative large distances, up to about $R \sim 0.7fm$. At very large distances, on the other hand, we expect that $H(\vec{R},t)$ is represented with some accuracy by the quenched approximation. We must switch from one correlation function to the other when using the quenched approximation, since we have to put in the breaking of the string by hand. Obviously, the quenched approximation does not have much to say about the intermediate regime.

The asymptotic behavior of the correlation function $H(\vec{R},t)$ is given by the mass in the static approximation. So we define the string breaking distance R_b by

$$V(R_b) = 2\tilde{M}_P, \tag{5.4}$$

with $V(R)$ being the quenched potential including the self-energy term that cancels in eq.(5.4). R_b defined in this way, gives an upper bound to the distance where the potential starts deviating significantly from the form of eq.(4.9).

From eq.(4.9) with $G(\vec{R}/a) \simeq a/(4\pi R)$, we can calculate R_b

$$R_b = (\tilde{M}_P - \frac{1}{2}V_0)/\sigma + \sqrt{[(\tilde{M}_P - \frac{1}{2}V_0)/\sigma]^2 + \frac{\pi}{12\sigma}} \tag{5.5}$$

As table 3 does not show any significant finite size effects on $\tilde{M}_P$ within the whole range of $1.5 \leq L\sqrt{\sigma} \leq 4.5$, we can safely neglect finite size effects on R_b. We have extrapolated $\tilde{M}_P$ at $L\sqrt{\sigma} \simeq 3$ linearly in $1/\kappa$ and calculated R_b at κ_s and κ_u. The results are listed in Table 8. Figure 13 shows the a dependence and our extrapolation to $a = 0$. For all quark masses, the continuum value is at $R_b = 4/\sqrt{\sigma}$ with about 10% statistical error. We estimate an uncertainty for the extrapolation in a of 10%, since the a-dependence is rather steep and end up with

$$R_b = 1.9(2)(2)fm \tag{5.6}$$

for all quark masses $m_q < 2m_s$.

Such distances are difficult to reach in a potential calculation including dynamical fermions. It should be noted, however, that the screening of the potential is expected

to appear at distances that are rather independent of the dynamical quark mass and hence can be observed with relatively large quark masses [13].

6. Summary and Conclusions

In this work we have investigated in detail the various aspects of the static approximation. We summarize here the main outcome of this study:

1. In order to filter out the ground state before noise sets in, one must use extended fermion fields. By varying the trial wave functions at $\beta = 6.26$ we found that extended plateaus in the local masses occur for wave functions with r.m.s. radius of about 0.3 fm. Using wave function with larger or smaller radii, the quality of the plateaus deteriorates. In particular for the local-smeared correlators the quality of the plateaus depends crucially on the choice of a good trial wave function. For the very small or large wave functions the plateaus set in at larger times where errors become significant. For these wave functions we can safely identify the region of the plateau only by using our knowledge of the height of the plateau deduced from looking at the smeared-smeared correlator. If we then fit in the range of the identified plateau we arrive at results which are all consistent and stable under variation of the time interval of the fit. The error bars are smallest for the best wave function. The results are insensitive to a change of shape of the trial wave functions of given r.m.s. radius. We therefore conclude that the results for the decay constant in the static approximation are stable under variations of the size and shape of the trial wave functions as long as plateaus are correctly identified in the manner discussed in section 3. This corroborates our previous findings [4].

2. Having established the wave function independence of the decay constant we studied scaling, using the best wave function at each value of β. We find that for $L \gtrsim 1.5$ fm the volume dependence of f is negligible. Using results at a fixed volume of about $(1.5 \text{ fm})^3$ we observe the a-dependence to be rather strong when the mass of the ρ meson is used to set the scale. If, on the other hand, the physical scale is based on the string tension the a-dependence turns out to be much weaker. In other words, at small β values one is faced with significant effects from the choice of scale. After continuum extrapolation, however, both alternatives are observed to yield identical results within error bars. But the latter are considerably reduced in the string tension option.

3. In our original calculation of f [3] we anticipated systematic errors arising from the renormalisation constant Z_{stat}, the choice of physical scale and the $a \to 0$ extrapolation. Here we have carried out the $a \to 0$ extrapolation and found a

[13] Note that the significant change compared to the numbers given in ref. [37], is due to a copying mistake in that reference.

10% correction due to the scale and a 13% correction due to the renormalisation constant Z_{stat}. All these corrections act in the same direction, i.e. they lower the estimate for f. As a consequence, we finally end up with [14]

$$f_{bd} = 230(22)(26)MeV, \qquad f_{bs} = 266(17)(30)MeV.$$

4. In the mass range of the D-meson there is a substantial difference between the result for f obtained in the static approximation and using propagating heavy quarks, which points to large $1/M_P$ corrections.

5. The plateau of the local mass for the scalar correlator is not as wide as for the pseudoscalar. This means that the result for the scalar-pseudoscalar splitting Δ_S is less conclusive than for the pseudoscalar mass. We do not observe a definite dependence on the light quark mass. Extrapolating to $a = 0$ our results at light quark mass twice the strange quark we estimate

$$\Delta_S = 344(37)MeV.$$

For Λ_b the situation is even less clear and more study is required to establish a reliable estimate.

6. From our quenched calculation we are able to produce an upper bound for the distance where string breaking should occur in the full QCD. After extrapolating to $a = 0$ we obtain

$$R_b = 1.9(2)(2)fm.$$

We do not observe a strong dependence on the light quark when we vary from the chiral limit to quarks of mass twice the strange quark mass.

Acknowledgements: We have benefited from discussions with O. Pene and E. Eichten whom we also thank for communicating his new (preliminary) results to us.

These calculations were carried out on the NEC-SX3 at the Supercomputing Center in Manno, Switzerland and on the CRAY-Y-MP in Jülich, Germany. We thank both institutions for their generous support.

[14] After completion of this work we became aware of the most recent (preliminary) data from the Fermilab group, presented by Eichten at the Amsterdam *Lattice '92* conference. They are in agreement with our data at the largest value of the light quark mass. However they appear to differ by 25% after linear extrapolation to the chiral point. We are unable, at this point, to give a conclusive explanation for the discrepancy.

7. Appendix A: Simulation Parameters

We work in the quenched approximation, using the standard Wilson formulation [38, 39] of the lattice action

$$S = S_G + S_F \tag{7.1}$$

with

$$S_G(U) = \beta \sum_x \sum_{\mu>\nu} \{1 - \frac{1}{6} \mathrm{Re\ Tr}\ P_{\mu\nu}(x)\} \tag{7.2}$$

and

$$\begin{aligned} S_F(\bar{\Psi}, \Psi, U) = \sum_x \{ \frac{1}{2\kappa} \bar{\Psi}(x)\Psi(x) - \frac{1}{2} \sum_\mu [\ & \bar{\Psi}(x)(1-\gamma_\mu)U_\mu(x)\Psi(x+a\hat{\mu}) \\ & + \ \bar{\Psi}(x)(1+\gamma_\mu)U_\mu^\dagger(x)\Psi(x-a\hat{\mu}) \ ] \} \\ = \bar{\Psi} M \Psi \quad . \end{aligned} \tag{7.3}$$

Here, as in most of the following, we have suppressed Dirac and color indices. a denotes the lattice constant and $P_{\mu\nu}(x)$ is the product of gauge parallel transporters $U_\mu(x) \in$ SU(3) around an elementary plaquette and is given by

$$P_{\mu\nu}(x) = U_\mu(x) U_\nu(x + a\hat{\mu}) U_\mu^\dagger(x + a\hat{\nu}) U_\nu^\dagger(x) \quad . \tag{7.4}$$

The gauge fields are periodic functions of x, and the fermion fields Ψ are taken periodic in space over a length L and antiperiodic in time over a time extent L_t. The hopping parameter κ is related to the bare quark mass m by

$$\kappa = \frac{1}{2(ma+4)} \quad . \tag{7.5}$$

In order to quantify finite a and finite size effects, the calculations have been performed on a series of lattices which differ in the coupling constant β and in the lattice size L. In table 1 we give the parameters and nomenclature for the various lattices. The physical lattice spacing and size of the lattice, obtained by fixing the string tension σ to the value $(420\mathrm{MeV})^2$, are given in the last two columns.

Our Monte Carlo procedure employs a hybrid over-relaxation algorithm [40] to produce independent gauge configurations. In this algorithm N almost microcanonical over-relaxation sweeps [41] through the lattice are followed by one standard Metropolis sweep[42]. This combination is called one iteration. We separated our measurements by 100 iterations with N=1 at $\beta = 5.74$, 200 iterations with N=2 at $\beta = 6.0$ and 150 iterations with N=3 at $\beta = 6.26$.

As demonstrated in section 3.1, in order to obtain a reliable signal for the correlation functions and thus for the physical quantities of interest, we must smear the hadronic fields. This requires calculating the product of a finite-mass quark propagator S with smearing wave function $\Phi(x, x_4)$. This product is given by the solution of

$$\sum_y M(x,y)[\sum_z S(y,z)\Phi(z,x_4)] = \Phi(x,x_4) \quad , \tag{7.6}$$

where M is the fermion matrix of eq.(7.3). The linear equation (7.6) is preconditioned through an even-odd partitioning of the matrix [43] and then solved by the minimal residual algorithm [44]. In order to speed up the process further, the solution at the respectively higher quark mass is used as starting guess in the algorithm. For the quark masses used in this calculation, this combination saves a factor of 2-4 in cpu time compared to the standard conjugate gradient method. The accuracy needed in the matrix inversion is determined by testing the convergence of *all* correlation functions that are used in the calculation.

Let us briefly comment on the error analysis of the simulation results. We have generally binned our results into groups of up to 5 measurements, keeping, however, a minimum of around $N_{bin} = 20$ bins. As to be expected, no significant bin-size dependence of the statistical errors was found for the simulation parameters given above. The statistical error of a function $F(P^1, ..., P^r)$ of quantities P^i that are simple averages over configurations, was calculated using

$$\Delta(F) = \frac{1}{\sqrt{N_{bin}}} \sqrt{\sum_{i,j=1}^{r} \frac{dF}{dP^i} \, \mathrm{cov}(P^i, P^j) \, \frac{dF}{dP^j}} \quad , \tag{7.7}$$

with the covariance matrix given by

$$\mathrm{cov}(P^i, P^j) = \frac{1}{N_{bin}} \sum_{k=1}^{N_{bin}} (P_k^i - \bar{P}^i)(P_k^j - \bar{P}^j) \quad . \tag{7.8}$$

P_k^i is the average of P^i in the k^{th} bin. This procedure was applied e.g. for the time-dependent masses discussed in section 3.1. Statistical errors of parameters originating from fits to correlation functions or ratios of correlation functions as well as from fits extrapolating in mass were always determined by the use of the jackknife method [45] (with binning to control autocorrelations).

8. Appendix B: Variance of "local-smeared" correlators

In the following, we consider the variance of the correlations $C_\Gamma^{l,l;I,l}(t)$ and $C_\Gamma^{l,l;l,I}(t)$. Under two assumptions we derive an inequality which corresponds to the behavior of fig. 2.

As we calculate the real part of the correlation functions, there are two contributions (one from the operator squared, one from the operator times its adjoint). Since the discussion is completely identical for the two terms we write only the first one in the following. In the case where we smear the light quark on the "source side" this is given by

$$\begin{aligned} \sigma_1^2\{C_\Gamma^{l,l;l,I}(t)\} \; &= \qquad\qquad (8.1) \\ &\sum_{\vec{x},\vec{y}} < \mathcal{M}_{\Gamma,1}^{l,l}(\vec{x},t) \; [\mathcal{M}_{\Gamma,1}^{l,I}(\vec{0},0)]^\dagger \mathcal{M}_{\Gamma,2}^{l,l}(\vec{y},t) \; [\mathcal{M}_{\Gamma,2}^{l,I}(\vec{0},0)]^\dagger > - [C_\Gamma^{l,l;l,I}(t)]^2 \\ &= < \mathcal{M}_{\Gamma,1}^{l,l}(\vec{0},t) \; [\mathcal{M}_{\Gamma,1}^{l,I}(\vec{0},0)]^\dagger \mathcal{M}_{\Gamma,2}^{l,l}(\vec{0},t) \; [\mathcal{M}_{\Gamma,2}^{l,I}(\vec{0},0)]^\dagger > - [C_\Gamma^{l,l;l,I}(t)]^2 \quad , \end{aligned}$$

Here we have added a flavor index 1,2 to the quark fields: $\mathcal{M}^{I,J}_{\Gamma,i}(\vec{x},t) = \bar{h}^I_i(\vec{x},t)\,\Gamma\,l^J_i(\vec{x},t)$. It keeps track of the proper contractions of quark fields in eq. (8.2)[15]. It can be shown that

$$\sigma^2\{C^{l,l;l,I}_\Gamma(t)\} = \sigma^2\{C^{I,l;l,l}_\Gamma(t)\} = \sigma^2\{C^{l,I;l,l}_\Gamma(t)\}. \tag{8.2}$$

We proceed by expressing the first part of the variance through the eigenstates of the transfer matrix. States $|B_1(\vec{0})B_2(\vec{0})>$ with two static mesons (with different flavors) at $\vec{x}=0$ contribute. Denoting the energy of these states by $\exp(-E^{BB}_n(\vec{0}))$, we obtain

$$\sigma^2_1\{C^{l,l;l,I}_\Gamma(t)\} \;+\; [C^{l,l;l,I}_\Gamma(t)]^2 = \sum_{\vec{x},\vec{y}}\sum_n \exp(-E^{BB}_n(\vec{0})\;t)\;\gamma(\vec{y},\vec{x})\;, \tag{8.3}$$

$$\begin{aligned}\gamma(\vec{y},\vec{x}) \;&=\; \gamma(\vec{x},\vec{y}) = <0|\mathcal{M}^{l,l}_{\Gamma,1}(\vec{0},t)\;\mathcal{M}^{l,l}_{\Gamma,2}(\vec{0},t)|n;B_1(\vec{0})B_2(\vec{0})> \\ &\quad <n;B_1(\vec{0})B_2(\vec{0})|\bar{l}_1(\vec{y})F^I(\vec{y},\vec{0};\mathcal{U}(0))\;\Gamma\;h_1(\vec{0})\;\;\bar{l}_2(\vec{x})F^I(\vec{x},\vec{0};\mathcal{U}(0))\;\Gamma\;h_2(\vec{0})|0>\end{aligned} \tag{8.4}$$

Correspondingly we have

$$\begin{aligned}\sigma^2_1\{C^{l,l;I,l}_\Gamma(t)\} \;+\; &[C^{l,l;I,l}_\Gamma(t)]^2 = \\ &\sum_{\vec{x},\vec{y}} <\mathcal{M}^{l,l}_{\Gamma,1}(\vec{x},t)\;[\mathcal{M}^{I,l}_{\Gamma,1}(\vec{0},0)]^\dagger \mathcal{M}^{l,l}_{\Gamma,2}(\vec{y},t)\;[\mathcal{M}^{I,l}_{\Gamma,2}(\vec{0},0)]^\dagger> \\ =\;&\sum_{\vec{x},\vec{y}} <\mathcal{M}^{l,l}_{\Gamma,1}(\vec{x},t)\;\bar{l}_1(\vec{0},0)F^I(\vec{0},\vec{x};\mathcal{U}(0))\;\Gamma\;h_1(\vec{x},0) \\ &\mathcal{M}^{l,l}_{\Gamma,2}(\vec{y},t)\;\bar{l}_2(\vec{0},0)F^I(\vec{0},\vec{y};\mathcal{U}(0))\;\Gamma\;h_2(\vec{y},0)>\;,\end{aligned} \tag{8.5}$$

$$\sigma^2_1\{C^{l,l;I,l}_\Gamma(t)\} \;+\; [C^{l,l;l,I}_\Gamma(t)]^2 = \sum_{\vec{x},\vec{y}}\sum_n \exp(-E^{BB}_n(\vec{x}-\vec{y})\;t)\;\alpha(\vec{y},\vec{x})\;, \tag{8.6}$$

$$\begin{aligned}\alpha(\vec{y},\vec{x}) \;&=\; \alpha(\vec{x},\vec{y}) = <0|\mathcal{M}^{l,l}_{\Gamma,1}(\vec{x})\;\mathcal{M}^{l,l}_{\Gamma,2}(\vec{y})|n;B_1(\vec{x})B_2(\vec{y})> \\ &\quad <n;B_1(\vec{x})B_2(\vec{y})|\bar{l}_1(\vec{0})F^I(\vec{0},\vec{x};\mathcal{U})\;\Gamma\;h_1(\vec{x})\;\;\bar{l}_2(\vec{0})F^I(\vec{0},\vec{y};\mathcal{U})\;\Gamma\;h_2(\vec{y})|0>\end{aligned} \tag{8.7}$$

For large values of t, the expressions for σ^2 are dominated by the $n=1$ contribution. Let us assume that $E^{BB}_1(\vec{x})$ increases with $\vec{x}^2$, i.e. that the interaction between the static mesons is attractive. Then $\exp(-E^{BB}_1(\vec{x}-\vec{y})\;t) \simeq \delta_{\vec{x}\vec{y}}\;\exp(-E^{BB}_1(\vec{0})\;t)$ in the limit of large t. Since $\alpha(\vec{x},\vec{x}) = \gamma(\vec{x},\vec{x})$ we obtain (in the limit of large t)

$$\sigma^2_1\{C^{l,l;l,I}_\Gamma(t)\} - \sigma^2_1\{C^{l,l;I,l}_\Gamma(t)\} \simeq \exp(-E^{BB}_1(\vec{0})\;t)\sum_{\vec{x}\neq\vec{y}}\gamma(\vec{y},\vec{x})\;. \tag{8.8}$$

Since we are using wave functions without nodes, $\gamma(\vec{y},\vec{x})$ is expected to be positive for all $\vec{x},\vec{y}$. The second contribution to the variance is identical to the above except that we have B_1–$\bar{B}_2$ correlation functions instead of B_1–B_2.

Therefore – accepting the above assumption – we arrive at the conclusion that (at large t) the variance of the correlation function can be reduced if we smear the heavy quark on the "source side" compared to the other cases. In fig. 2, this effect is there for all values of t, which is expected following the argument given above if one assumes that $E^{BB}_n(\vec{x})$ increases with $\vec{x}^2$ for general n.

[15]This is necessary since we want to calculate the variance of the observable that is defined *after* we have integrated out the fermion fields.

References

[1] B. Grinstein, Nucl. Phys. B339 (1990) 253; H. Georgi and M. B. Wise, Phys. Lett. B243 (1990) 279; N. Isgur and M. B. Wise, Phys. Lett. B237 (1990) 527.

[2] E. Eichten, in *"Field Theory on the Lattice"*, Nucl. Phys. B (Proc.Suppl.) 4 (1988) 147.

[3] C. Alexandrou, S. Güsken, F. Jegerlehner, K. Schilling, and R. Sommer, Phys. Lett. B256 (1991) 60.

[4] C. Alexandrou, S. Güsken, F. Jegerlehner, K. Schilling, and R. Sommer, Nucl. Phys. B374 (1992) 263.

[5] C.R. Allton et al., Nucl. Phys. B349(1991)598.

[6] C. Bernard, J. Labrenz, and A. Soni, in *"Lattice 90"*, Nucl. Phys. B (Proc. Suppl.) 20 (1991) 488.

[7] S. Hashimoto and Y. Saeki, Hiroshima University preprint HUPD-9120 and Nucl. Phys. B (Proc. Suppl.) 26 (1992) 381.

[8] E. Eichten, G. Hockney, and H. B. Thacker, in *"Lattice 89"*, Nucl. Phys. B (Proc. Suppl.) 17 (1990) 529.

[9] E. Eichten, G. Hockney, and H. B. Thacker, in *"Lattice 90"*, Nucl. Phys. B (Proc. Suppl.) 20 (1991) 500.

[10] S. Güsken, in *"Lattice 89"*, Nucl. Phys. B (Proc. Suppl.) 17 (1990) 361

[11] E. Eichten and F. Feinberg, Phys. Rev. D 23 (1981) 2724.

[12] M. Lüscher, Comm. Math. Phys. 54 (1977) 283.

[13] N. Isgur and M. B. Wise, Phys, Lett. B232 (1989) 113

[14] E. Eichten, in *"Lattice 90"*, Nucl. Phys. B (Proc. Suppl.) 20 (1991) 475.

[15] R. Sommer, C. Alexandrou, S. Güsken, F. Jegerlehner, and K. Schilling, in *"Lattice 91"*, Nucl. Phys. B (Proc. Suppl.) 26 (1992) 387.

[16] M. Bochicchio, G. Martinelli, C. R. Allton, C. T. Sachrajda, and D. B. Carpenter, Nucl. Phys. B 372 (1992)403.

[17] G. Parisi, in *"High-Energy Physics —1980"*, XX. Int. Conf., Madison (1980), ed. L. Durand and L.G.Pondrom (American Institute of Physics, New York, 1981).

[18] G.P. Lepage and P.B. Mackenzie, Nucl. Phys. B(Proc. Suppl.) 20 (1991) 173 and Fermilab preprint 91/355-T.

[19] M. Lüscher, R. Sommer, U. Wolff, and P. Weisz, CERN preprint CERN-TH 6566/92.

[20] G.S. Bali and K. Schilling, Wuppertal University preprint WUB-92-29, to appear in Phys. Rev D.

[21] G.P. Lepage and B.A. Thacker in *"Field Theory on the Lattice"*, Nucl. Phys. B (Proc. Suppl.) 4 (1988) 199.

[22] C. Davies and B. Thacker, in *"Lattice 91"*, Nucl. Phys. B (Proc. Suppl.) 26 (1992) 375 and 378

[23] G.P. Lepage, in *"Lattice 91"*, Nucl. Phys. B (Proc. Suppl.) 26 (1992) 45; G. P. Lepage and P. B. Mackenzie, *"On the Viability of Lattice Perturbation Theory"*, Cornell/FERMILAB preprint, Sept. 1992.

[24] Ph. Boucaud, C. L. Lin, and O. Pene, Phys. Rev. D40 (1989) 1529 + erratum.

[25] Ph. Boucaud, J. P. Leroy, J. Micheli, O. Pene, and G. C. Rossi, CERN preprint CERN-TH-6599-92

[26] G.S. Bali and K. Schilling, Phys. Rev. D46 (1992) 2636; the values quoted here have been reanalysed by G. Bali using eq.(4.9).

[27] Analysis of R. Sommer of the MTC-data, K.D. Born it et al., Nucl. Phys. B (Proc. Suppl.) 20 (1991) 394.

[28] M. Lüscher, Nucl. Phys. B180 (1981) 317

[29] The APE group, Phys. Lett. B 214 (1988) 115, Nucl. Phys. B (Proc. Suppl.) 20 (1991) 399, Nucl. Phys. B (Proc. Suppl.) 26 (1992) 278.

[30] see e.g. J. Gasser and H. Leutwyler, Phys. Rep. C87 (1982) 77.

[31] L. H. Karsten and J. Smit, Nucl.Phys. B183 (1981) 103.

[32] T. Yoshie et al., in *"Lattice 91"*, Nucl. Phys. B (Proc. Suppl.) 26 (1992) 281; we would like to thank Y. Iwasaki for communicating raw data from this computation; this data confirms the nonlinearities that we observed.

[33] C. Michael and M. Teper, Nucl. Phys. B314(1989)347.

[34] See fig. 4 of C. Bernard, J. Labrenz, and A. Soni, Nucl. Phys. B (Proc. Suppl.) 20 (1991) 488.

[35] T.M. Aliev and V. L. Eletsky, Sov. J. Nucl. Phys. 38 (1983) 936; S. Narison, Phys. Lett. 198B (1987) 104.

[36] E. Laermann et al., Nucl. Phys. B (Proc. Suppl.) 26 (1992) 268.

[37] R.Sommer, C. Alexandrou, S. Güsken, F. Jegerlehner, and K. Schilling, Nucl. Phys. B (Proc. Suppl.) 20 (1991) 493.

[38] K. G. Wilson, Phys. Rev. D10 (1974) 2445.

[39] K. G. Wilson, in *New Phenomena in Subnuclear Physics*, Erice 1975, Plenum, New York (1977).

[40] M. Creutz, Phys. Rev. D36 (1987)515; F. R. Brown and T. J. Woch, Phys. Rev. Lett. 58 (1987)2394.

[41] R. Gupta, G. W. Kilcup, A. Patel, S. P. Sharpe, and P. De Forcrand, Mod. Phys. Lett. A3, (1988)1367.

[42] N. Metropolis, M. W. Rosenbluth, M. N. Rosenbluth, A. H. Teller, and E. Teller, J. Chem. Phys. 21 (1953)1087.

[43] R. Gupta et. al. Phys. Rev. D 40 (1989) 2072.

[44] S. C. Eisenstat, H. C. Elman, and M. H. Schultz, Siam. J. Number. Anal. Vol.20, No 2, April 1983.

[45] see for example S. Gottlieb, P. B. Mackenzie, H. B. Thacker, and D. Weingarten, Nucl. Phys. B263 (1986) 704.

Table Captions

Table 1: Parameters of the lattices used for this work. The inverse lattice spacing and the spatial extension L in physical units are obtained from fixing the string tension to $(420MeV)^2$.

lattice	β	$L/a,\ L_t/a$	no. config's.	a^{-1}/GeV	L/fm
A1	5.74	4, 24	404	1.12	0.70
A2	5.74	6, 24	131		1.06
A3	5.74	8, 24	170		1.41
A3a	5.74	8, 24	100		1.41
A4	5.74	10, 24	213		1.76
A5	5.74	12, 24	140		2.12
B1	5.82	6, 28	100	1.32	0.90
C1	6.00	6, 36	227	1.88	0.63
C2	6.00	8, 36	100		0.84
C3	6.00	12, 36	204		1.26
C3a	6.00	12, 36	100		1.26
C4	6.00	18, 36	27		1.89
D1	6.26	12, 48	103	2.78	0.85
D2	6.26	18, 48	33		1.28
D2a	6.26	18, 48	43		1.28

Table 2: Bare decay constant and mass in lattice units, using the static approximation for the $18^3 \times 48$ lattice at $\beta = 6.26$ and $\kappa = 0.1492$. The smallest time separation in the correlators used for the fit is given by t_{min}/a and the largest is fixed at $t_{max}/a = 17$. An asterisk $(*)$ indicates that the fit was not accepted due to either the missing of a plateau in the local masses in the region of the fit or a value of χ^2 larger than the one to be expected including the correlations of the data.

α n	r_1/a	r_2/a	$a\tilde{M}_P$	$t_{\rm min}/a$	$a^{3/2}\hat{F}/Z_{stat}$
loc+gaus	2.5	3.9	0.569(7)	2	0.235(19)*
				4	0.223(18)*
				6	0.213(18)*
				8	0.208(20)
				10	0.205(21)
				12	0.203(24)
loc+gaus	3.5	4.6	0.566(7)	2	0.221(19)*
				4	0.211(19)*
				6	0.204(20)*
				8	0.200(21)
				10	0.198(22)
				12	0.195(25)
loc+gaus	4.1	5.0	0.566(7)	2	0.216(19)*
				4	0.208(19)*
				6	0.201(20)*
				8	0.198(20)
				10	0.196(22)
				12	0.192(25)
4 70	4.2	4.6	0.566(7)	2	0.201(15)*
				4	0.200(15)*
				6	0.198(18)
				8	0.195(18)
				10	0.194(20)
				12	0.190(22)
4 100	5.2	5.6	0.565(8)	2	0.188(15)*
				4	0.190(16)*
				6	0.190(17)
				8	0.189(20)
				10	0.188(21)
				12	0.185(25)
5 160	6.1	6.5	0.566(8)	2	0.170(13)*
				4	0.176(15)*
				6	0.180(18)
				8	0.181(20)
				10	0.181(21)
				12	0.180(24)

Table 3: Bare decay constant and mass in lattice units, using the static approximation. An asterisk (*) indicates that the fit was not accepted due to a large χ^2 or the missing of a plateau in the local masses in the region of the fit. A dagger (†) indicates that smearing was applied to both heavy and light quarks.

latt.	κ	K	α n	r_2/a	$a^{3/2}\hat{F}/\ Z_{stat}$					$a\tilde{M}_P$
					$t_{min}=2a$	$t_{min}=3a$	$t_{min}=4a$	$t_{min}=5a$	$t_{min}=6a$	
A1	0.1560		2.0 10	1.8	0.751(35)*	0.770(51)	0.781(66)	0.788(74)		0.834(28)
A1	0.1580		2.0 10	1.8	0.751(33)*	0.771(50)	0.785(63)	0.791(69)		0.833(27)
A2	0.1560		2.0 10	2.6	0.775(31)*	0.798(46)	0.810(60)	0.817(65)		0.833(27)
A2	0.1580		2.0 10	2.6	0.757(31)*	0.774(47)	0.784(61)	0.789(65)		0.811(29)
A3	0.1560		2.0 10	2	*	0.840(31)*	0.919(46)	0.882(43)	0.900(46)	0.855(17)
A3	0.1620		2.0 10	2	*	0.769(33)*	0.785(41)	0.798(43)	0.811(41)	0.785(21)
A3	0.1635		2.0 10	2	*	0.745(31)*	0.756(39)	0.766(39)	0.780(34)	0.768(20)
A3a	0.1560	0.1866			0.874(16)	0.884(26)	0.879(29)	0.884(59)		0.837(5)
A3a	0.1600	0.1866			0.840(18)	0.836(26)	0.822(29)	0.829(64)		0.792(5)
A3a	0.1620	0.1866			0.819(25)	0.808(35)	0.794(44)	0.803(78)		0.772(6)
A3a	0.1635	0.1866			0.805(33)	0.790(43)	0.772(56)	0.780(95)		0.758(8)
A4	0.1560		2.0 10	3.6	0.782(22)*	0.809(35)*	0.829(43)	0.841(50)	0.835(54)	0.831(21)
A4	0.1580		2.0 10	3.6	0.765(25)*	0.788(36)	0.804(44)	0.813(51)	0.804(55)	0.810(23)
A5	0.1560		2.0 10		0.777(19)*	0.809(33)*	0.854(42)	0.834(46)	0.840(49)	0.841(18)
A5	0.1620		2.0 10		0.740(18)*	0.768(31)	0.781(40)	0.790(40)	0.793(37)	0.792(18)
A5	0.1635		2.0 10		0.719(22)*	0.760(44)	0.745(47)	0.748(50)	0.745(47)	0.779(20)
B1	0.1557	0.1856		1.9	*	0.635(60)	0.618(69)	0.590(81)		0.764(13)
B1	0.1574	0.1856		1.9	*	0.618(63)	0.596(71)	0.571(81)		0.749(15)
B1	0.1587	0.1856		1.9	*	0.609(72)	0.581(81)	0.558(98)		0.746(18)
C1	0.1525		4.0 50	3.8	0.313(19)	0.322(27)	0.326(33)	0.325(37)		0.646(28)
C2	0.1500		4.0 25	3.2	0.333(16)*	0.349(22)*	0.368(31)	0.376(50)		0.704(9)
C2	0.1525		4.0 25	3.2	0.351(18)	0.356(24)	0.364(37)			0.669(10)
C3	0.1525		4.0 50	4.0	0.345(10)*	0.365(18)*	0.379(24)	0.388(31)	0.397(43)	0.690(18)
C3	0.1540		4.0 50	4.0	0.330(10)*	0.347(16)*	0.360(29)	0.369(26)	0.375(37)	0.665(18)
C3	0.1558		4.0 50	4.0	0.316(15)*	0.334(24)*	0.346(30)	0.354(37)	0.365(47)	0.652(16)
C3a	0.1525	0.1854		4.0	*	0.451(06)*	0.415(14)*	0.394(19)	0.390(25)	0.687(12)
C3a	0.1540	0.1854		4.0	*	0.431(06)*	0.395(14)*	0.371(20)	0.369(26)	0.666(13)
C3a	0.1550	0.1854		4.0	*	0.416(08)*	0.381(14)*	0.359(20)	0.359(27)	0.653(14)
C4	0.1525		4.0 50†		*	0.353(14)*	0.361(16)*	0.368(18)	0.371(19)	0.672(14)
D1	0.1492		4. 100	5.0	0.190(11)*	0.195(14)	0.201(16)	0.206(20)	0.204(21)	0.541(31)
D2	0.1492		4. 100	5.5	0.203(09)*	0.211(11)*	0.214(13)	0.213(13)		0.598(33)
D2	0.1506		4. 100	5.5	0.190(09)*	0.196(11)*	0.198(11)	0.195(11)		0.575(31)
D2	0.1514		4. 100	5.5	0.184(10)*	0.189(11)*	0.188(11)	0.185(11)		0.565(31)
D2a	0.1492		4. 100	5.6	0.188(15)*	0.189(16)*	0.190(16)	0.190(18)	0.190(19)	0.565(8)

Table 4: The mass splittings Δ_S and Δ_Λ and the scale of string breaking R_b in lattice units are given. An asterisk indicates that no clear plateau could be identified. The second column gives the parameters for the gaussian trial wave functions used. For all lattices smearing was applied either to the heavy or light quark except for lattice C4 where both quarks were smeared. A dagger (†) denotes numbers obtained not by fitting the ratio R_S but separately the scalar and pseudoscalar correlators.

latt.	α n	κ	$a\Delta_S$	$a\Delta_\Lambda$	R_b/a
A3	2. 10	0.1560	0.431(20)	0.57(8)*	7.9(3)
	2. 10	0.1620	0.482(92)*	0.46(3)*	6.9(3)
	2. 10	0.1635	0.500(130)*	0.43(6)*	6.7(3)
A5	2. 10	0.1560	0.413(21)	0.35(9)*	7.7(3)
	2. 10	0.1620	0.435(32)	*	7.0(3)
	2. 10	0.1635	0.449(34)	*	6.8(3)
C3	4. 50	0.1525	0.210(12)	*	15.3(9)
		0.1540	0.196(21)	*	14.4(9)
		0.1558	0.136(86)	*	13.9(8)
C4	4. 50	0.1525	0.210(18)	0.326(8)	14.6(8)
D1	4. 100	0.1492	0.174(11)*	*	21(3)
D2	4. 100	0.1492	0.149(57)†	*	26(3)
	4. 100	0.1506	0.159(53)†	*	24(3)
	4. 100	0.1514	0.172(51)†	*	23(3)
D2a	4. 100	0.1492	0.142(18)	0.216(14)	23(1)

Table 5: Values for the constant piece of the quenched $Q\bar{Q}$ potential (eq. 4.9) and the String tension.

β	$a\ V_0$	$a^2\ \sigma$	Reference
5.70	0.631(3)	0.168(1)	[27]
5.74	0.636(5)	0.141(2)	interpolated
5.80	0.643(3)	0.109(1)	[27]
5.90	0.647(3)	0.073(2)	[27]
6.00	0.630(4)	0.050(1)	[26]
6.20	0.614(1)	0.0271(2)	[26]
6.26	0.607(2)	0.0229(3)	interpolated
6.40	0.589(1)	0.0154(1)	[26]

Table 6: The κ-values κ_c and κ_s corresponding to zero and strange quark mass are given for each β. In the two last columns we list the values of M_ρ in lattice units at κ_c and κ_s. The values of κ_s are obtained using M_ρ as a reference scale.

β	κ_c	κ_s	aM_ρ	aM_{ρ_s}
5.74	0.16631(19)	0.16194(15)	0.534(11)	0.660(8)
6.0	0.15716(14)	0.15493(12)	0.341(15)	0.427(10)
6.26	0.15234(12)	0.15139(9)	0.208(18)	0.263(14)

Table 7: We give the bare decay constant $\hat{F}$ / Z_{stat} and pseudoscalar mass in lattice units extrapolated at κ_c and at κ_s. The latter was fixed by using both M_ρ and the string tension (in square brackets) as a reference scale. The subscript u and s denote quantities evaluated at the chiral limit and at the strange quark mass respectively.

β	$a^{3/2}\hat{F}_u$ / Z^{stat}	$a\tilde{M}_{P_u}$	$a^{3/2}\hat{F}_s$ / Z^{stat}	$a\tilde{M}_{P_s}$
5.74	0.768(28)	0.730(8)	0.814(21)[0.843(17)]	0.774(5)[0.804(5)]
6.0	0.327(14)	0.627(8)	0.356(13)[0.369(13)]	0.655(11)[0.667(10)]
6.26	0.177(11)	0.550(30)	0.189(12)[0.198(12)]	0.565(31)[0.577(31)]

Table 8: The mass splittings Δ_S and Δ_Λ and the scale of string breaking R_b in lattice units are given at κ_c and at κ_s. The latter was fixed by using M_ρ and the string tension (in square brackets) as a reference scale. The notation is the same as in table 7.

β	$a\Delta_{S_u}$	$a\Delta_{\Lambda_u}$	R_{b_u}/a	$a\Delta_{S_s}$	$a\Delta_{\Lambda_s}$	R_{b_s}/a
5.74	0.516(29)	0.387(58)	6.15(19)	0.477(19)[0.450(16)]	0.462(39)[0.512(25)]	6.75(18)[7.16(19)]
6.0	0.211(20)		12.86(73)	0.217(15)[0.223(13)]		14.95(73)[14.39(67)]
6.26	0.179(49)		22(3)	0.169(51)[0.160(52)]		23(3)[24(3)]

Figure Captions

Figure 1: Local masses as defined in eq. (2.8) for the pseudoscalar meson in the static approximation on an $18^3 \times 48$ lattice at $\beta = 6.26$ and $\kappa = 0.1492$ are plotted versus the time separation, t, in lattice units. The diamonds denote the mass from the "local-local" correlation function. The data denoted by $G1, G2$ and $G3$ show the local mass for smeared-smeared correlators where the trial wave functions are combinations of a local and a gaussian function. The rest are gaussian trial wave functions, the smallest being the one with parameters $n = 70, \alpha = 4$ and the largest with $n = 160, \alpha = 5$.

Figure 2: Local masses from the "local-smeared" correlator for the pseudoscalar meson on an $18^3 \times 48$ lattice at $\beta = 6.26$ and $\kappa = 0.1492$. (i) (circles) denotes results with smearing applied to the static sink; (ii) (diamonds) presents results from a linear combination of a correlator with smearing applied to the static source and a correlator with smearing as in (i) . In both cases smearing was done using a gaussian wave function with $\alpha = 4, n = 100$.

Figure 3: Local masses from the "local-smeared" correlator for the pseudoscalar meson on an $18^3 \times 48$ lattice at $\beta = 6.26$ and $\kappa = 0.1492$, with smearing using six different wave functions listed in table 2. The notation for the wave functions is the same as fig. 2. The error band arising from fitting the "smeared-smeared" correlator for the best trial wave function is shown by the two dashed lines.

Figure 4: Local masses from "local-smeared" correlators for the pseudoscalar meson for lattices A3 and A5 at $\beta = 5.74$, C3 and C4 at $\beta = 6.0$ and D2a at $\beta = 6.26$ (see table 1) with the error band arising from fitting the corresponding "smeared-smeared" correlator. The light quark mass is fixed so that $M_P(l,l)/\sqrt{\sigma} \sim 4$.

Figure 5: Local masses from the ratio, R_S, of scalar to pseudoscalar "smeared-smeared" correlator for lattices A3, A5, C3, C4 and D2a for a light quark mass as in fig. 4. The time axis is in units of the string tension.

Figure 6: Local masses from the ratio, R_Λ, of scalar to pseudoscalar "smeared-smeared" correlator for lattices A3, C3 and D2a for a light quark mass the same as in fig. 4. Both the time axis and the mass splitting are in units of the string tension.

Figure 7: To determine κ_c and $a^{-1}_{M_\rho}$ at $\beta = 5.74$, 6.0 and 6.26, linear fits to $M^2_P(l,l')$ and $M_V(l,l')$ are shown, where l, l' stand for fully propagating quarks of mass $\leq 2m_{strange}$.

Figure 8: The ρ mass at the chiral limit is shown as a function of the lattice spacing both expressed in units of the string tension. The extrapolated value at $a = 0$ is obtained from the linear fit (dashed line) to the four data points.

Figure 9: The ratio of the pseudoscalar decay constant to the vector mass, $f_P(l,l')/M_V(l,l')$, is plotted as a function of $M^2_P(l,l')/M^2_V(l,l')$, where the meaning of l, l' is the same as in fig. 7. The stars denote the experimental value for the pion and kaon.

Figure 10: $\frac{1}{Z_{stat}}\hat{F}\sigma^{-3/4}$ is shown vs $L\sqrt{\sigma}$. The circles denote the results at $\beta = 6.26$ the squares at $\beta = 6.0$ and the diamonds at $\beta = 5.74$. The light quark mass was fixed at the same value as that in fig 4. The dashed line is the result of fitting all data to the form $C_0 - C\exp(-1.5L\sqrt{\sigma})$ with $C_0 = 3.64$ and $C = 4.27$.

Figure 11: Continuum extrapolation of $F = \frac{1}{Z_{stat}}\hat{F}$ at light quark mass equal to the strange quark mass (F_s) and at the chiral limit (F_u). The values at $a = 0$ emerge from the linear fits (dashed lines) to the data points at $\beta = 5.74, 6.0$ and 6.26. In (a) and (b) both F and a are given in units of the string tension and in (c) and (d) in units of the ρ mass.

Figure 12: Continuum extrapolation of the scalar-pseudoscalar mass splitting at twice the strange quark mass, Δ_{2s}. The values at $a = 0$ result from the linear fits (dashed lines) to the data at $\beta = 5.74, 6.0$ and 6.26. In (a) we use units set by the string tension and in (b) by the ρ mass.

Figure 13: The string breaking distance $R_b\sqrt{\sigma}$ is shown vs $a\sqrt{\sigma}$ for three light quark masses: in (a) at twice the strange quark mass, in (b) at the strange quark mass and in (c) at the chiral limit. Linear fits to the data at $\beta = 5.74, 6.0$ and 6.26 are shown by the dashed line together with the extrapolated values at $a = 0$.

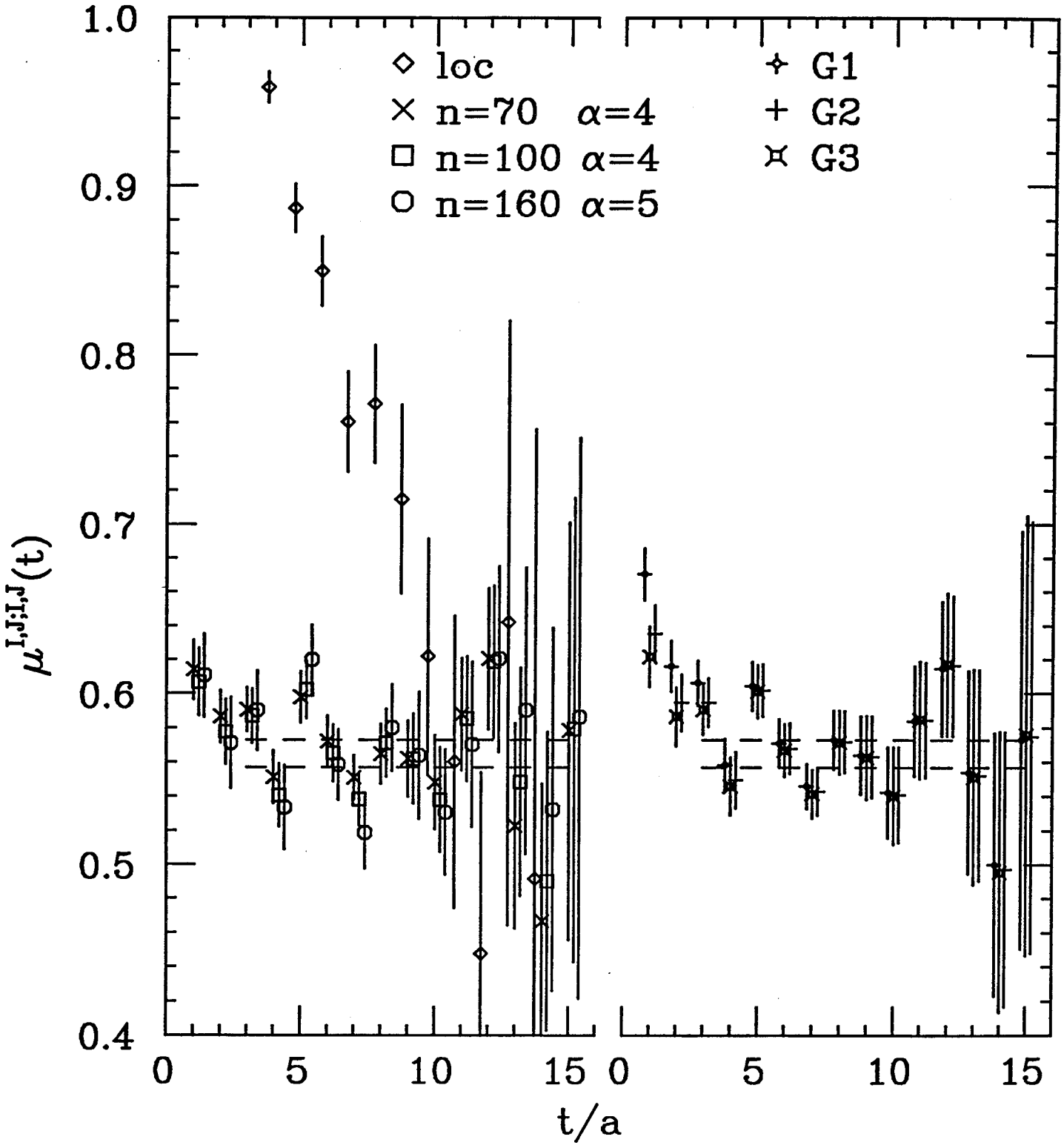
1.0
0.9
0.8
0.7
0.6
0.5
0.4
$\mu^{I,J;I,J}(t)$
loc
n=70 α=4
n=100 α=4
n=160 α=5
G1
G2
G3
0
5
10
15
t/a

Figure 1

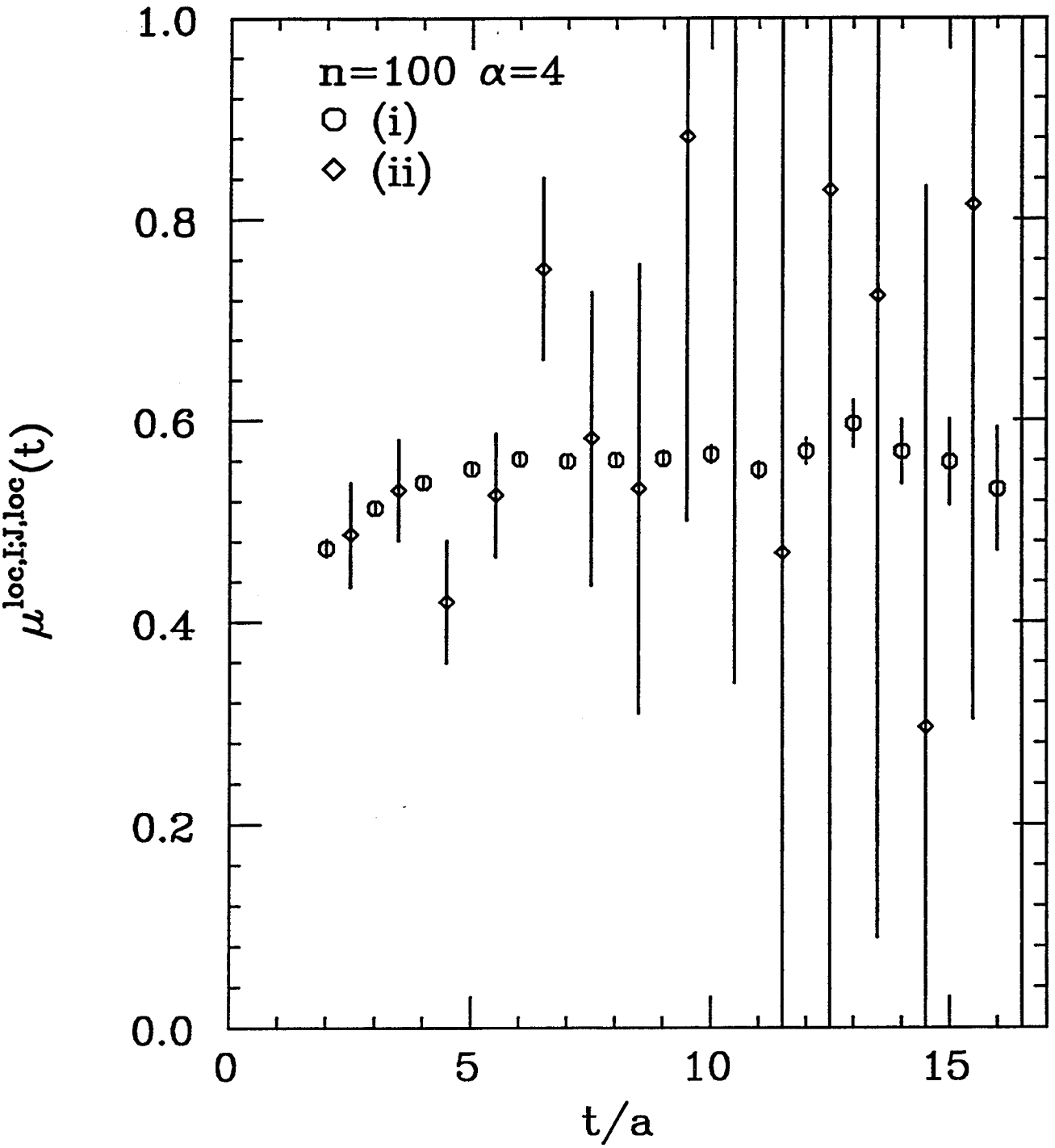

Figure 2

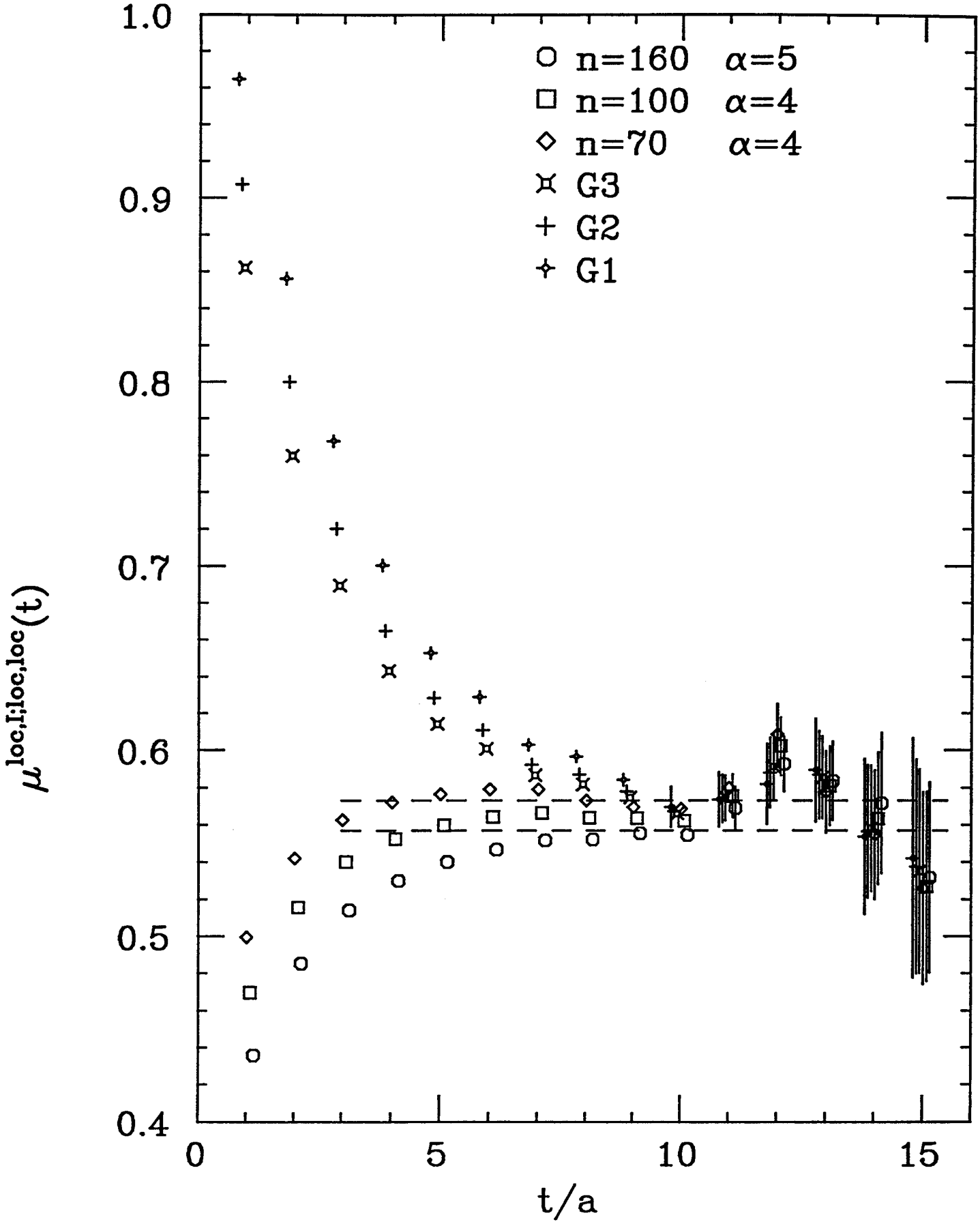
1.0
0.9
0.8
0.7
0.6
0.5
0.4
0
5
10
15
t/a
$\mu^{loc,I;loc,loc}(t)$
n=160 α=5
n=100 α=4
n=70 α=4
G3
G2
G1

Figure 3

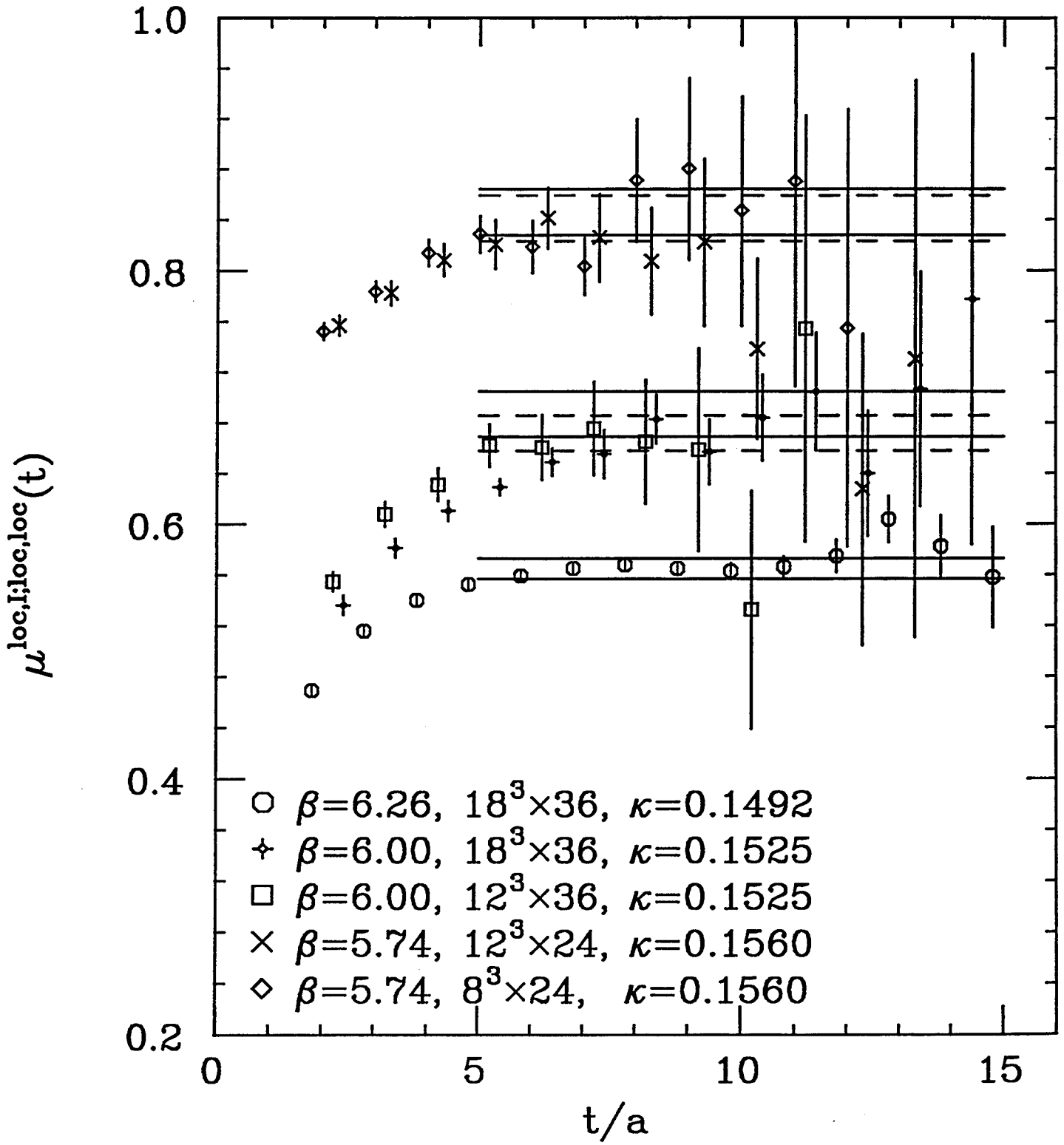
1.0
0.8
0.6
0.4
0.2
0
5
10
15
t/a
$\mu^{loc,I;loc,loc}(t)$
β=6.26, $18^3\times36$, κ=0.1492
β=6.00, $18^3\times36$, κ=0.1525
β=6.00, $12^3\times36$, κ=0.1525
β=5.74, $12^3\times24$, κ=0.1560
β=5.74, $8^3\times24$, κ=0.1560

Figure 4

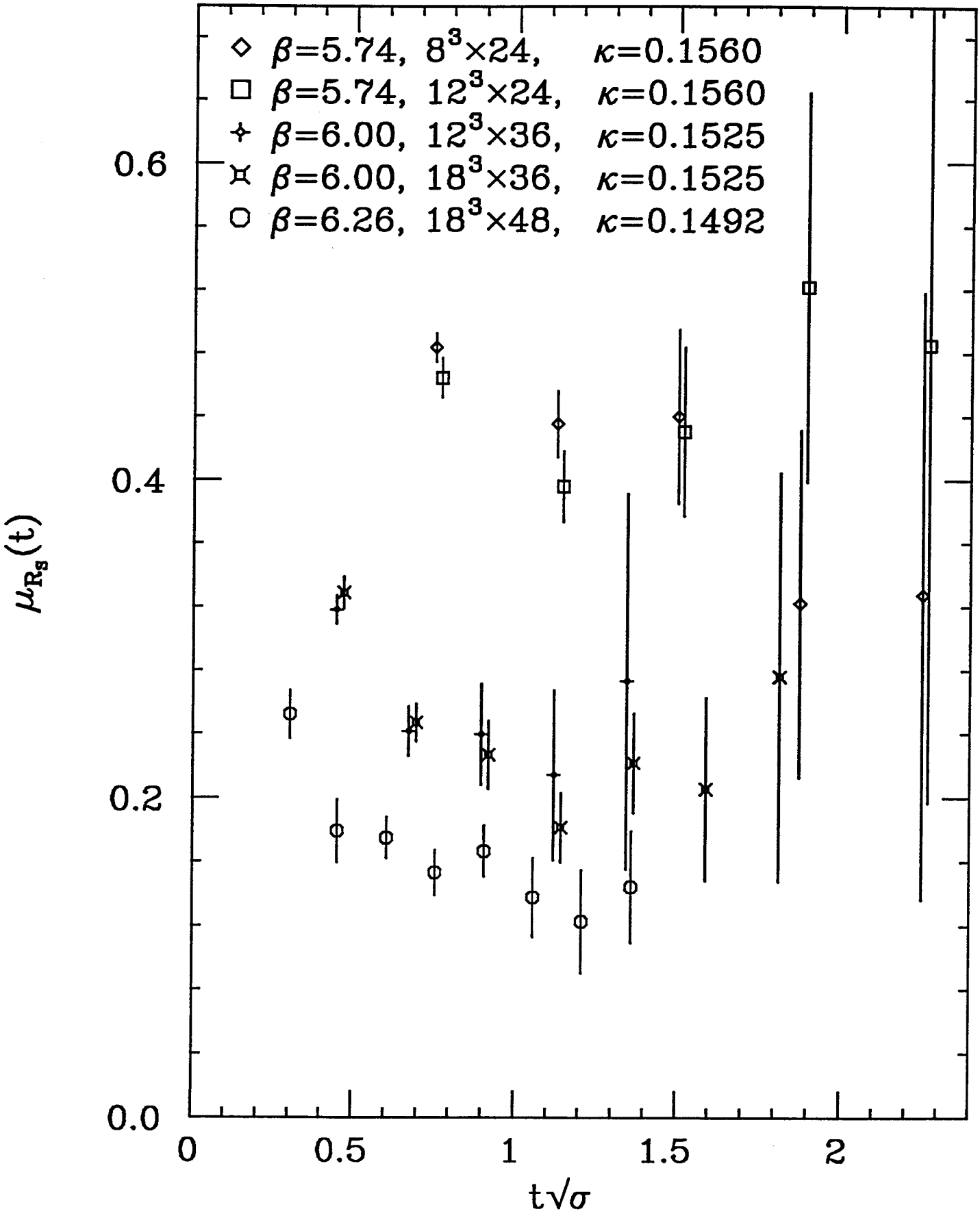
β=5.74, 8³×24, κ=0.1560
β=5.74, 12³×24, κ=0.1560
β=6.00, 12³×36, κ=0.1525
β=6.00, 18³×36, κ=0.1525
β=6.26, 18³×48, κ=0.1492
0.6
0.4
0.2
0.0
0
0.5
1
1.5
2
$\mu_{R_S}(t)$
$t\sqrt{\sigma}$

Figure 5

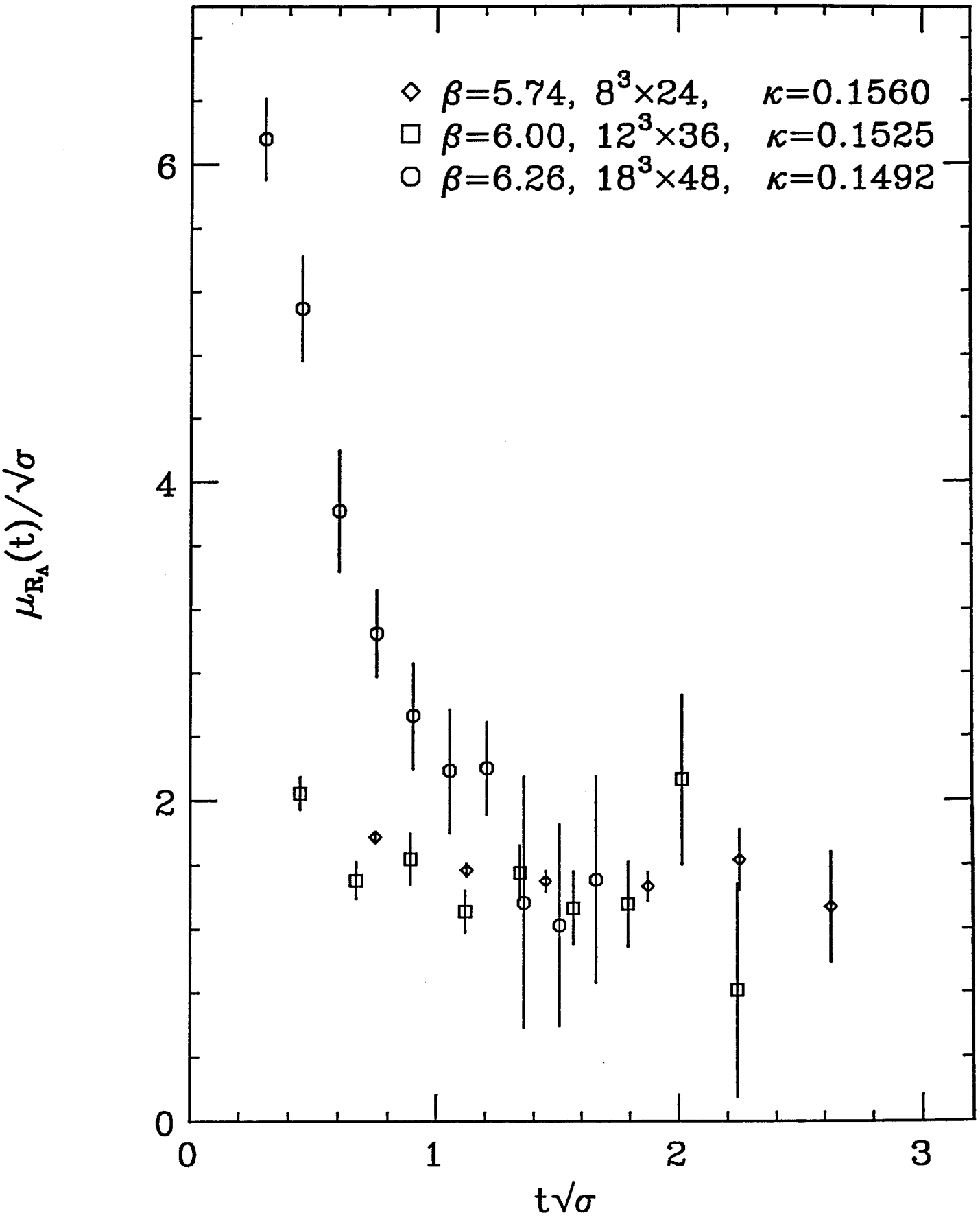
◇ β=5.74, 8³×24, κ=0.1560
□ β=6.00, 12³×36, κ=0.1525
○ β=6.26, 18³×48, κ=0.1492
$\mu_{R_A}(t)/\sqrt{\sigma}$
$t\sqrt{\sigma}$
0
2
4
6
0
1
2
3

Figure 6

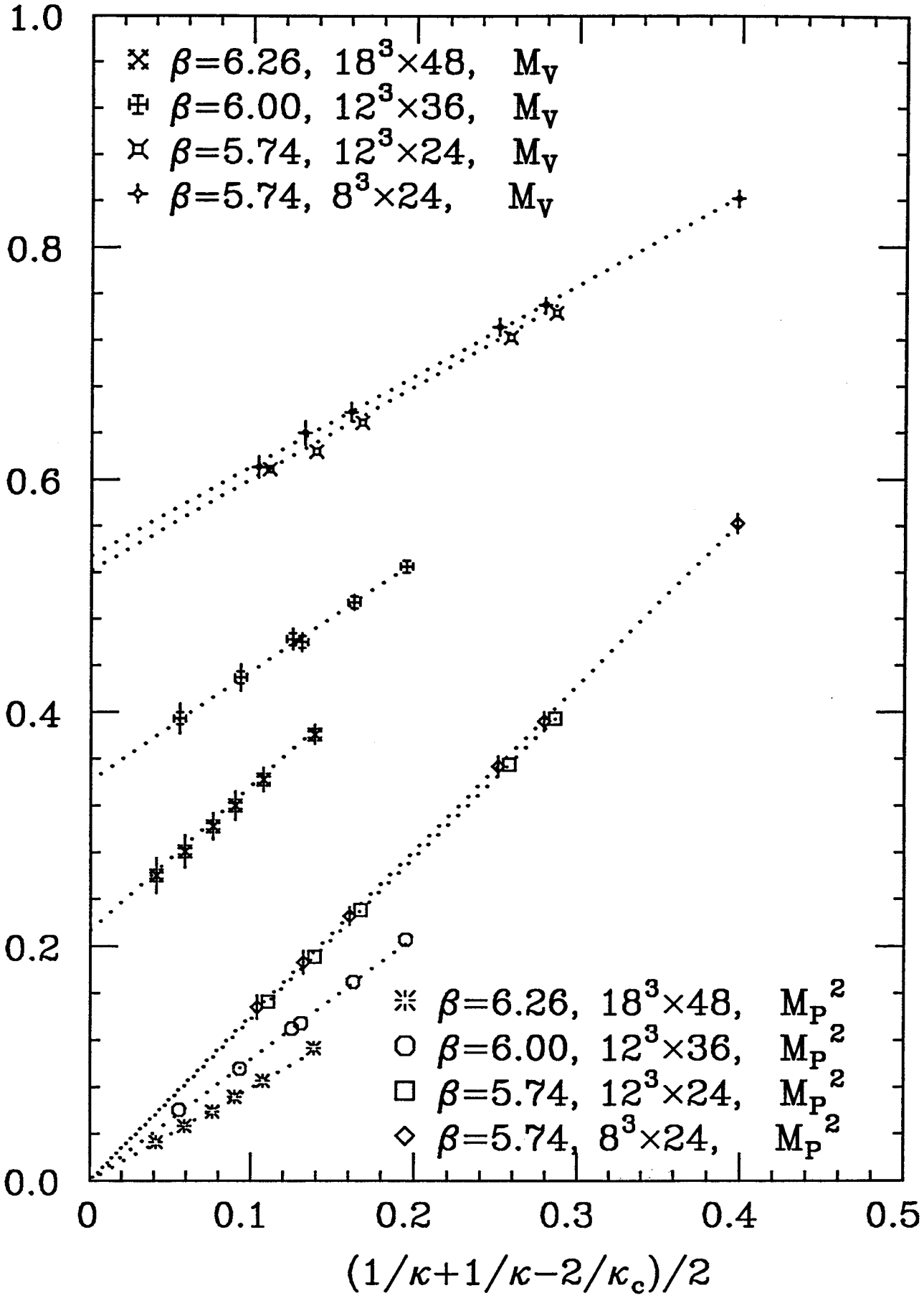
1.0
0.8
0.6
0.4
0.2
0.0
0
0.1
0.2
0.3
0.4
0.5
β=6.26, 18³×48, M_V
β=6.00, 12³×36, M_V
β=5.74, 12³×24, M_V
β=5.74, 8³×24, M_V
β=6.26, 18³×48, M_P²
β=6.00, 12³×36, M_P²
β=5.74, 12³×24, M_P²
β=5.74, 8³×24, M_P²
(1/κ+1/κ−2/κ_c)/2

Figure 7

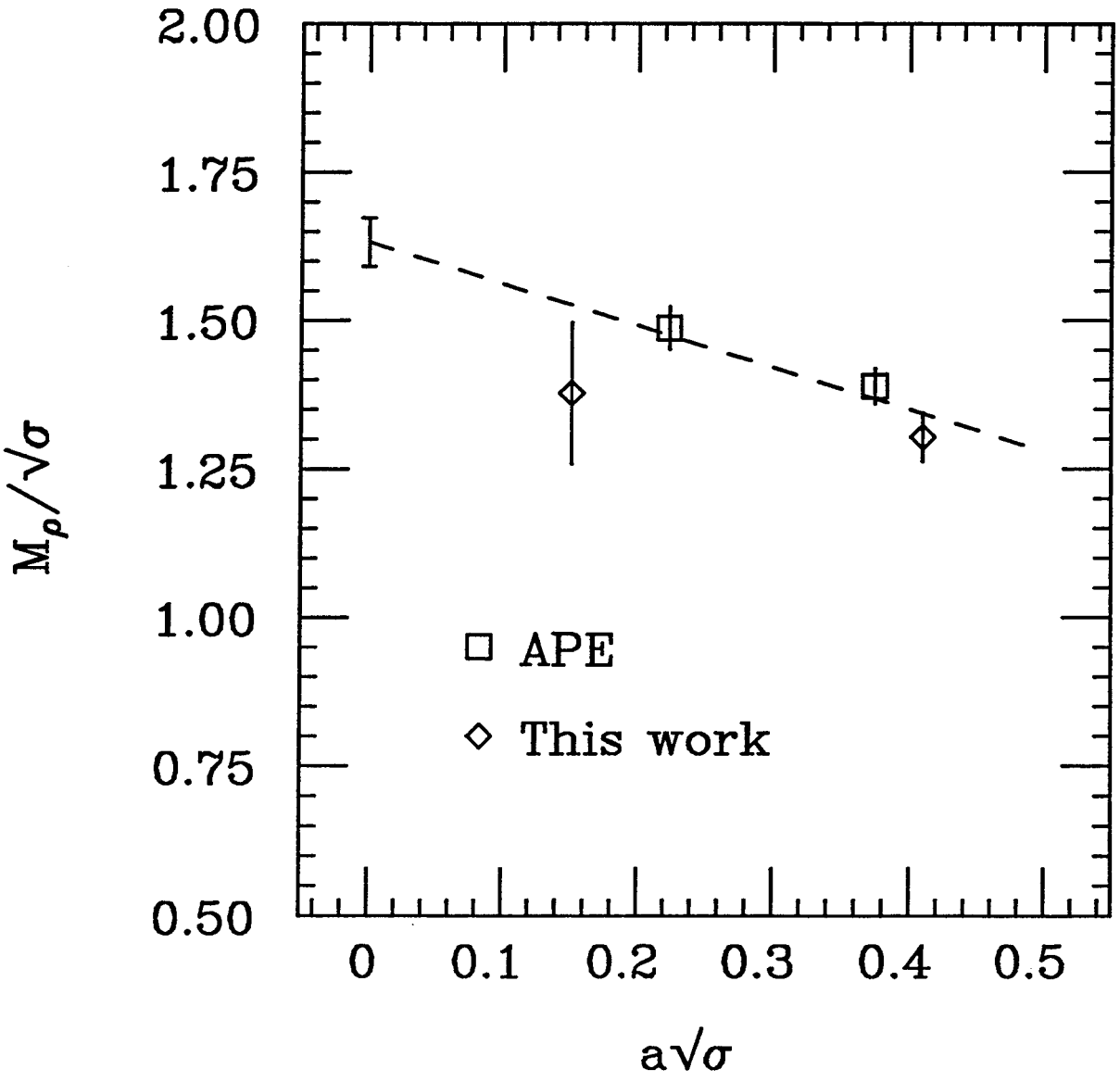
2.00
1.75
1.50
1.25
1.00
0.75
0.50
$M_\rho/\sqrt{\sigma}$
APE
This work
0
0.1
0.2
0.3
0.4
0.5
$a\sqrt{\sigma}$

Figure 8

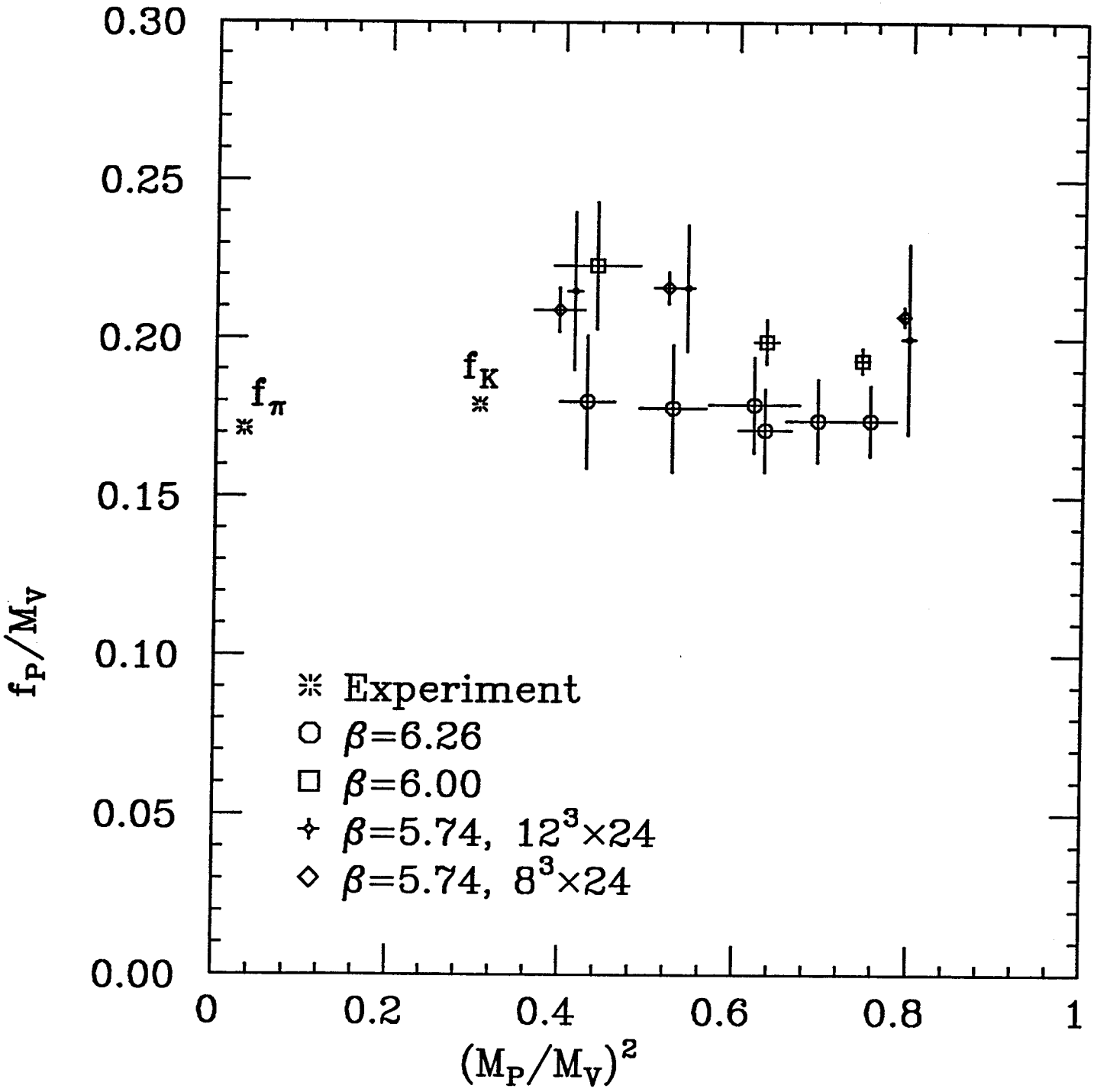
0.30
0.25
0.20
0.15
0.10
0.05
0.00
0
0.2
0.4
0.6
0.8
1
f_P/M_V
$(M_P/M_V)^2$
f_π
f_K
Experiment
β=6.26
β=6.00
β=5.74, $12^3\times24$
β=5.74, $8^3\times24$

Figure 9

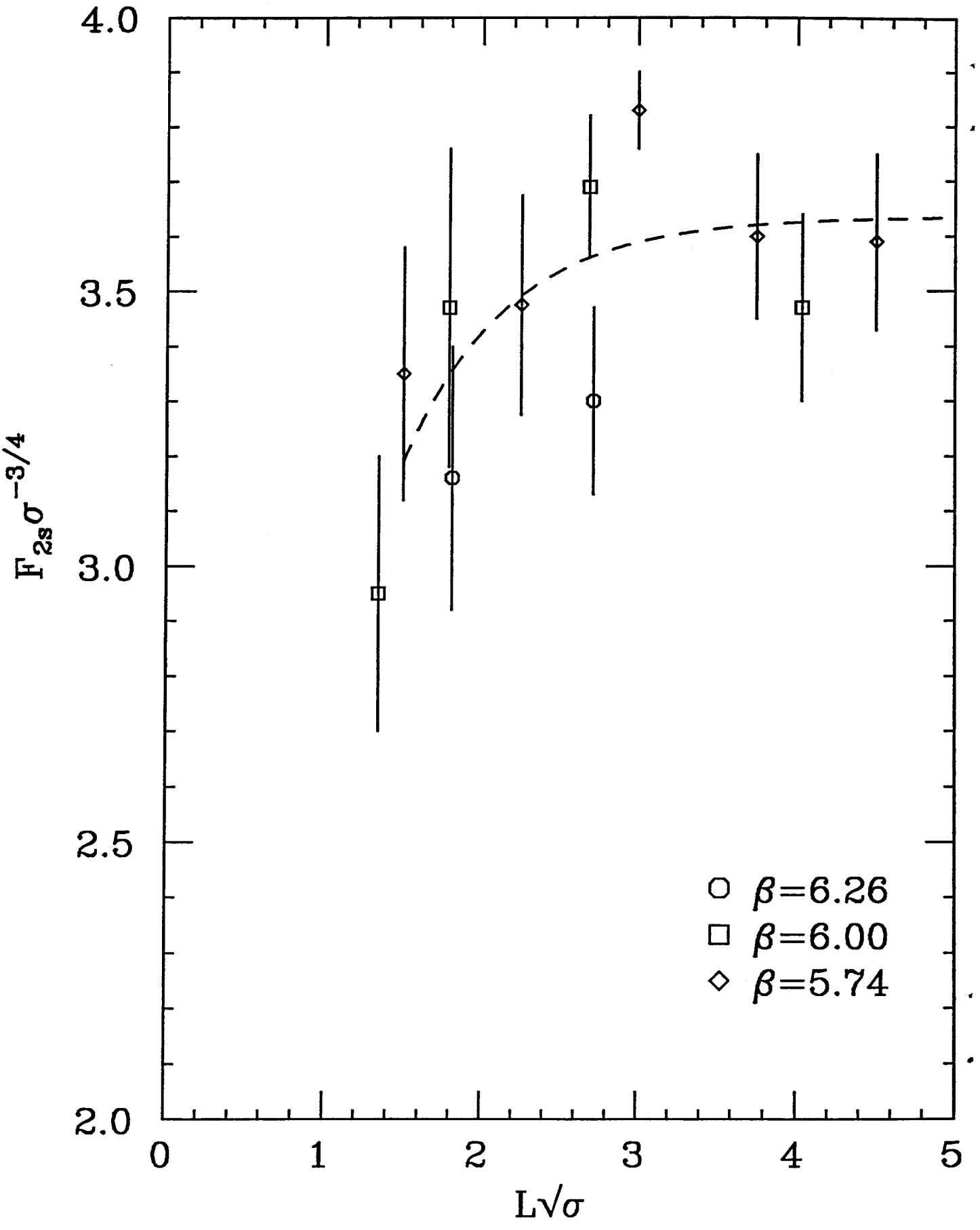
4.0
3.5
3.0
2.5
2.0
0
1
2
3
4
5
$F_{2s}\sigma^{-3/4}$
$L\sqrt{\sigma}$
β=6.26
β=6.00
β=5.74

Figure 10

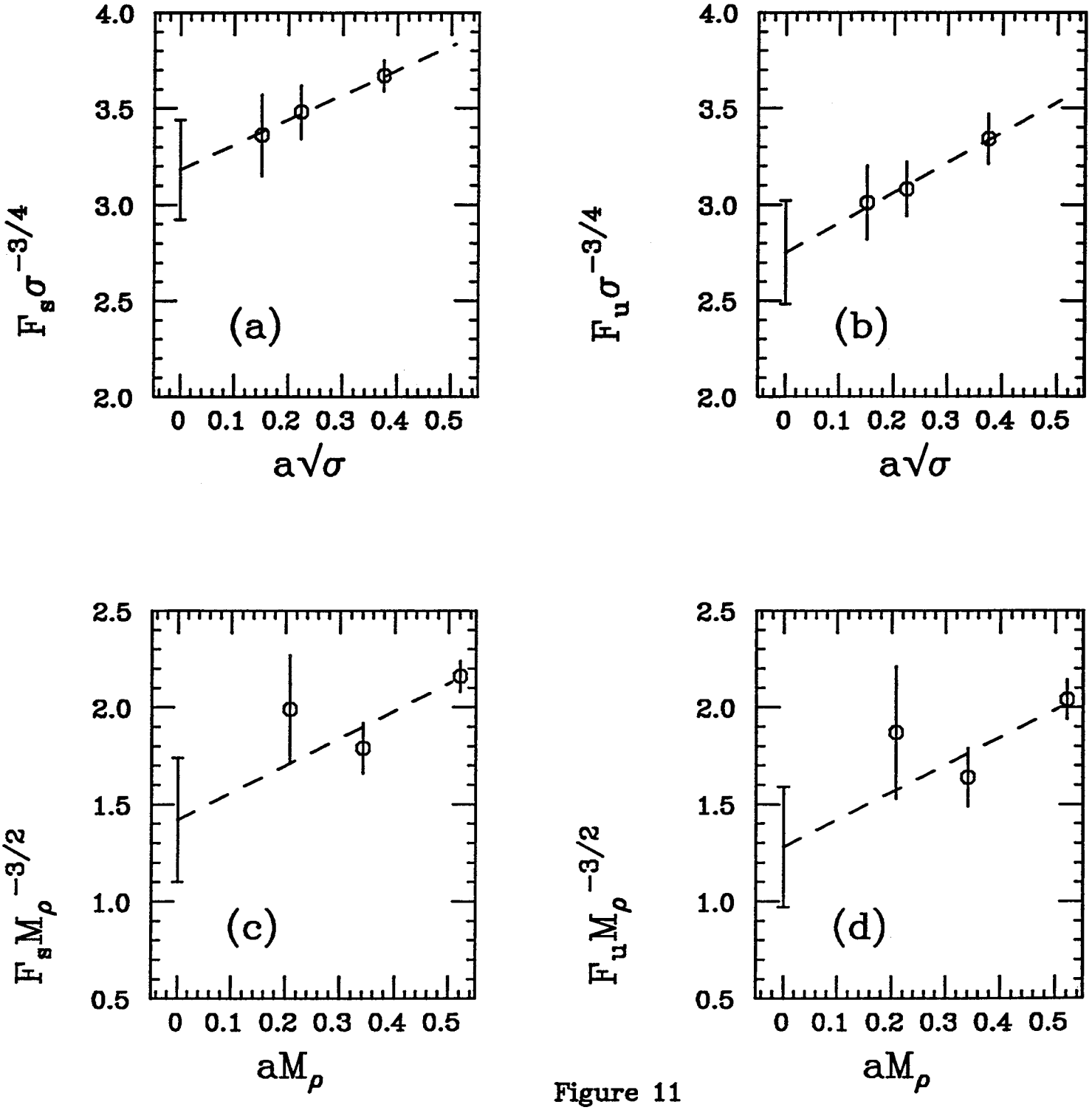
4.0
3.5
3.0
2.5
2.0
$F_s\sigma^{-3/4}$
(a)
0 0.1 0.2 0.3 0.4 0.5
$a\sqrt{\sigma}$
$F_u\sigma^{-3/4}$
(b)
$F_sM_\rho^{-3/2}$
2.5
2.0
1.5
1.0
0.5
(c)
aM_ρ
$F_uM_\rho^{-3/2}$
(d)

Figure 11

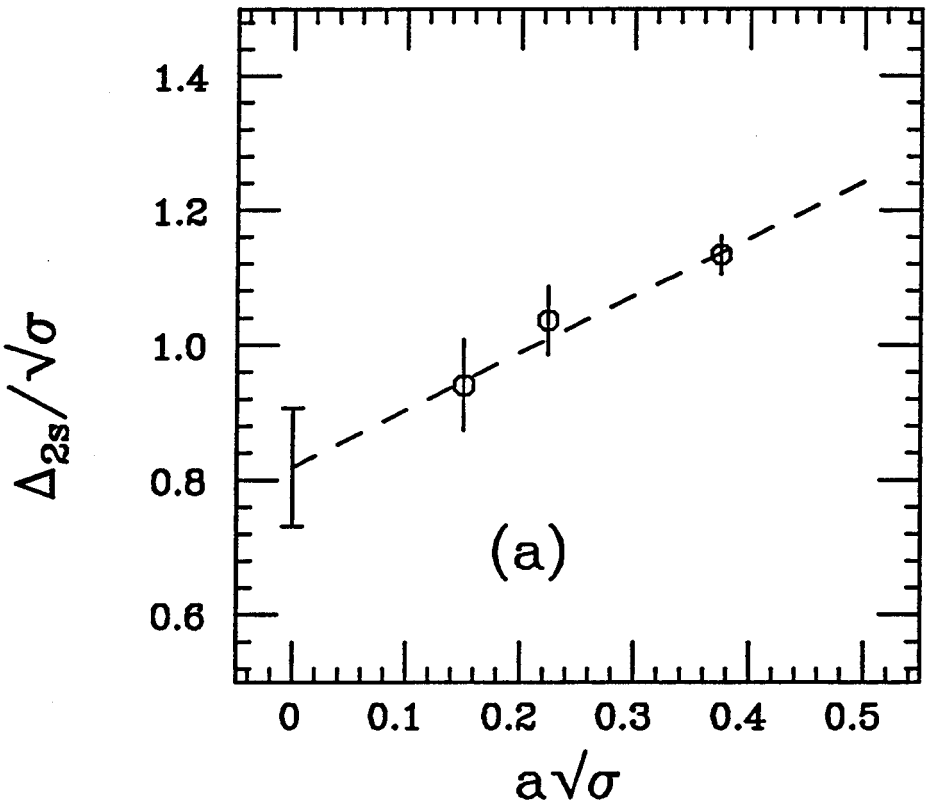
1.4
1.2
1.0
0.8
0.6
$\Delta_{2s}/\sqrt{\sigma}$
(a)
0
0.1
0.2
0.3
0.4
0.5
$a\sqrt{\sigma}$

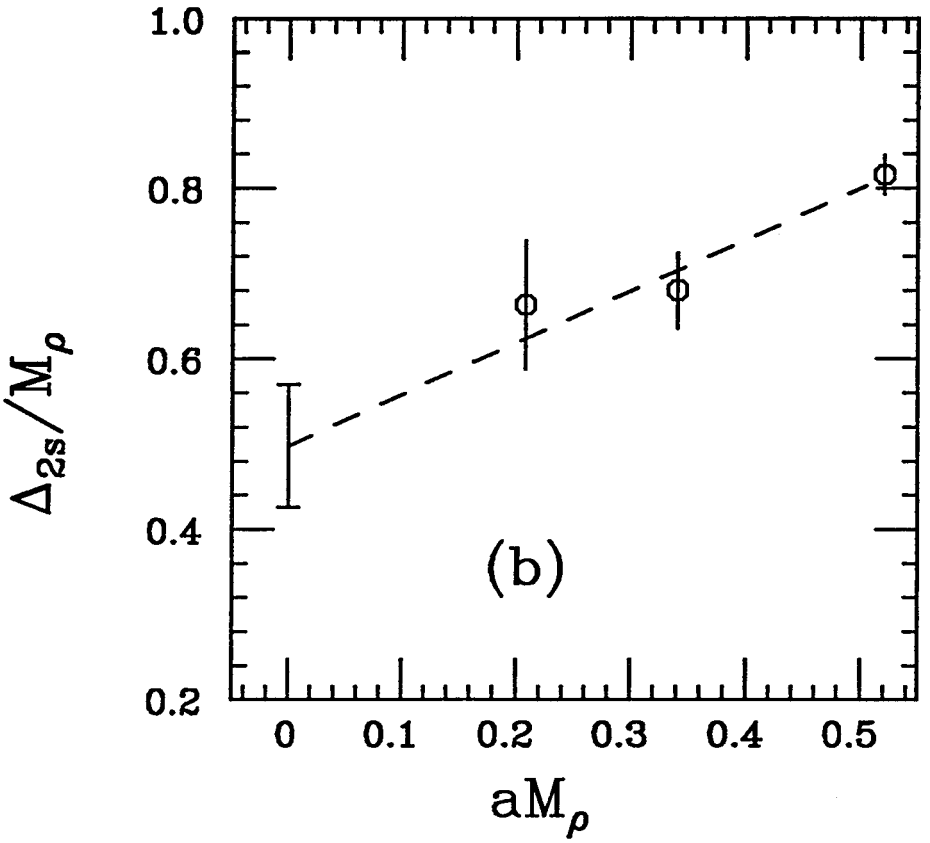
1.0
0.8
0.6
0.4
0.2
Δ_{2s}/M_ρ
(b)
0
0.1
0.2
0.3
0.4
0.5
aM_ρ

Figure 12

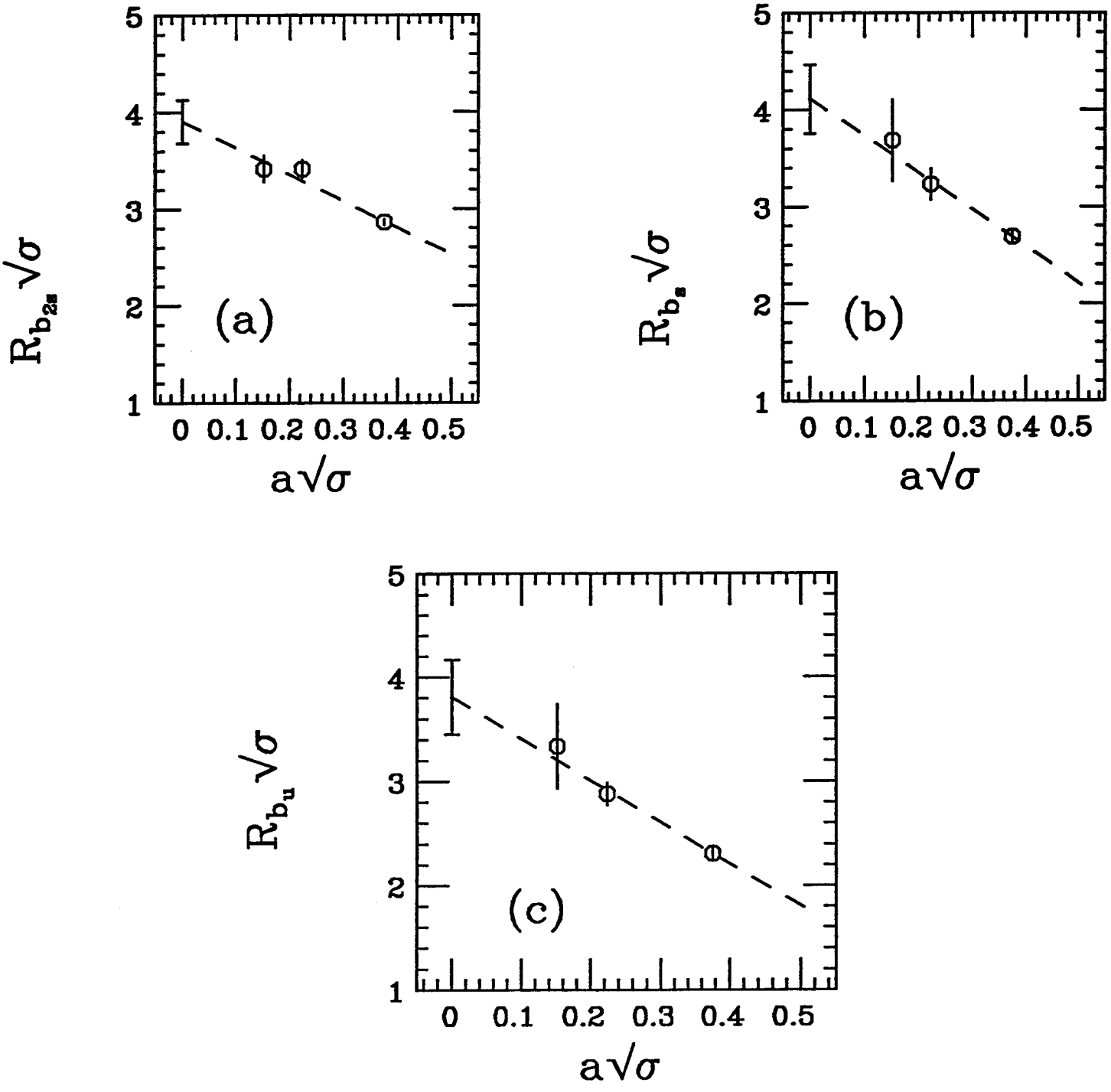
$R_{b_{2s}}\sqrt{\sigma}$
(a)
$a\sqrt{\sigma}$
$R_{b_s}\sqrt{\sigma}$
(b)
$a\sqrt{\sigma}$
$R_{b_u}\sqrt{\sigma}$
(c)
$a\sqrt{\sigma}$
0 0.1 0.2 0.3 0.4 0.5
1 2 3 4 5

Figure 13